UCLouvain

AGRO LOUVAIN

Faculté des bioingénieurs

Optimization of dual function materials (DFMs) for combined CO_2 capture and methanation

Author : Chloé Vandelois

Supervisors : Prof. Damien Debecker (UCLouvain/IMCN/MOST)
Dr. Plaifa Hongmanorom (UCLouvain/IMCN/MOST)

Readers : Prof. Eric Gaigneaux (UCLouvain/IMCN/MOST)
Prof. Vincent Dubois (LABIRIS)

Academic year 2022 - 2023

Master's degree in bioscience engineering: chemistry and bio-industries

Acknowledgements

I would like to thank all the people who supported me throughout the progress of this master thesis and without whom this work would not have been possible.

First of all, a particular thank you to my supervisor Pr. Damien Debecker for his guidance all along the way, as well as his availability and helpful advice. Many thanks also to my co-supervisor Dr. Plaifa Hongmanorom for her daily help and her ongoing involvement in my work.

I'd also like to thank François Devred for his daily guidance in the laboratory and his many words of advice, as well as the whole laboratory team for their warm welcome.

I would also like to thank Professors Eric Gaigneaux and Vincent Dubois for agreeing to be part of my thesis jury.

Finally, a warm thank you to my friends and family for their support and guidance throughout this thesis and more generally throughout my entire curriculum.

Abstract

Acting against climate change is one of the greatest challenges facing today's society. Greenhouse gas emissions are the main cause, leading to the emergence of a variety of solutions to mitigate them. Among these solutions, Dual Function Materials (DFMs) can both capture CO_2 and convert it into methane via its reaction with hydrogen. Allowing to produce a fuel that is both safer than hydrogen and carbon-neutral.

The properties of DFMs emerge from the simultaneous presence of basic and catalytic sites on the material. The proximity of these sites enhances reaction performance. Various compositions have been studied in the literature. In this work the DFM studied is 6%Na_2O-5%Ru/γ-Al_2O_3, synthesized via two successive wet impregnations.

This work focuses on the optimization of the DFM via two axes, the synthesis process and the composition. First, different calcination temperatures were tested for ruthenium impregnation. The objective was to understand the impact of calcination temperature on dispersion and Ru particle size and its impact on catalytic performance of the resulting DFM. Then the effect of ruthenium loading was tested.

To characterize the samples, N_2 physisorption, XRD, CO_2 TPD and in situ DRIFTS measurements were carried out. For each sample, a catalytic testing was carried out to test their performance in converting CO_2 to methane using a MS setup.

Our results show that higher calcination temperature favors bigger particle size but catalytic testing shows that calcination temperature and particle size only has a marginal impact on catalytic performances. Concerning Ru loading, better performances are observed for higher Ru loadings.

Contents

List of tables

List of figures

1 Introduction

1.1 Context

The industrial revolution (around 1850) and the changes in terms of fossil energy consumption, land use, consumption patterns and production that goes with it have led to climate warming. Indeed, over the period 2011-2019 an increase of around 1.1°C was observed compared to the period 1850-1900 [1,2] as seen in Figure 1.

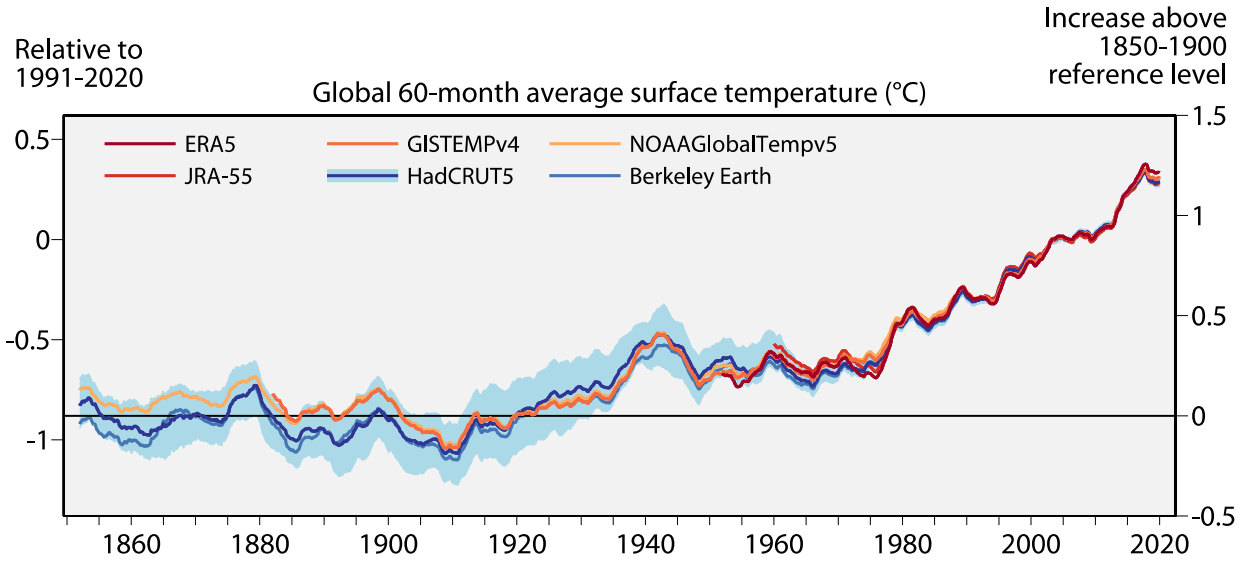

Figure 1 : Global surface temperature increase from 1850 to 2020 [2]

This increase in temperature is impacting the climate around the world, affecting food and water security as well as human health and economy. It is therefore becoming increasingly urgent to act and limit climate change. It has been estimated by the IPPC that the global temperature increase compared to the pre-industrial period should be limited to +1.5°C in order to avoid irreversible losses in biodiversity and repetitive crises in vulnerable communities [3].

To achieve this goal, it is first necessary to understand what causes global warming. It has been shown that greenhouse gases (GHGs) emissions, in particular CO_2 and methane, linked to human activities are the main drivers [3]. It would be necessary to reach carbon neutrality by 2050 if we want to respect the 1.5°C limit (objective included in the Paris Agreement) [4]. Unfortunately, the combustion of fossil resources used as fuels and the activity of some industries (e.g. cement, steel, etc. [5]) continues to generate massive amounts of CO_2 (

Figure 2). It is therefore urgent to find solutions as soon as possible to curb emissions and reduce the concentration of GHGs already emitted. As industrial emissions represent 64% of global CO_2 emissions, it is relevant to find solutions to reduce this specific type of emissions [6].

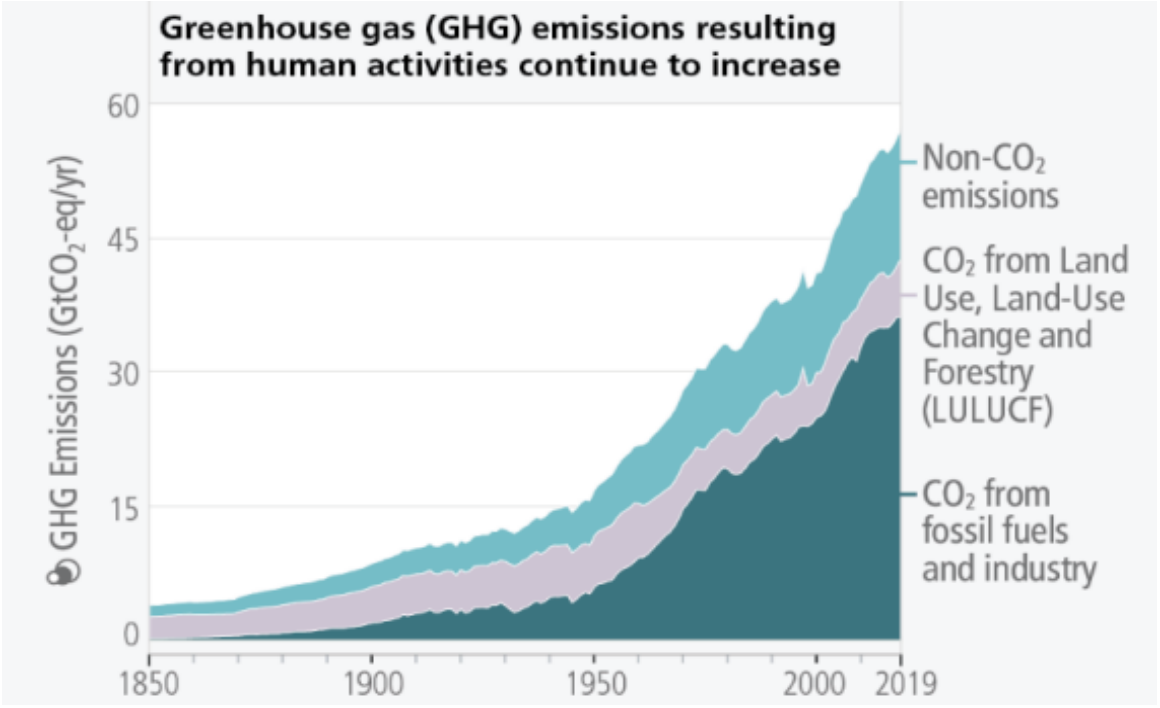

Figure 2 : Increase in CO_2 emissions from 1850 to 2019 [1]

1.2 Possible solutions

As mentioned above, it is necessary to reduce CO_2 emissions, especially from the industry, to reach carbon neutrality by 2050. For this purpose, different solutions exist. First, alternative energies can substitute fossil fuels and avoid/decrease CO_2 emissions. However, fossil fuels are not always replaceable or are not the source of emissions, in the case where CO_2 is a by-product of a reaction. It is then possible to capture CO_2 directly at the source (directly from industrial effluents for example) or even from ambient air (= Direct Air Capture, DAC). This CO_2 can then be either stored (= Carbon Capture and Storage, CCS) or transformed into another molecule (= Carbon Capture and Utilization, CCU) [7]. In addition to these technological solutions, it seems necessary to adopt a transformation in our consumption patterns in order to facilitate this energy transition.

1.2.1 Alternative energies to fossil fuels: renewable energies

The so-called renewable energies include solar power, wind power, hydropower, geothermal power and the biomass use. These energies becoming more and more competitive in terms of cost with fossil energies they have seen their use increase in recent years. Wind power, for example, is now among the cheapest new power plant technologies to provide electricity [8] and by 2050, clean energies could account for 65% of total power generation [9].

The main negative point of these technologies is their strong dependence on their environment and weather conditions, making them intrinsically intermittent modes of energy production and requiring the storage of the surplus energy produced [10]. This makes it difficult to rely on a single technology. The key to maximizing the use of renewable energy is therefore diversification: to combine the different types of existing technologies [11].

1.2.2 CCS and CCU

Both technologies capture CO_2 directly from a point source (such as a power plant) to avoid emissions. It is also possible to capture CO_2 directly from ambient air. This is known as Direct Air Capture (DAC) [12]. In the case of CCS, CO_2 is stored on the long term whereas in the case of CCU it is converted to valuable products. In both cases several capture methods and ends are possible, an overview of the different possibilities is summarized in Figure 3 [13].

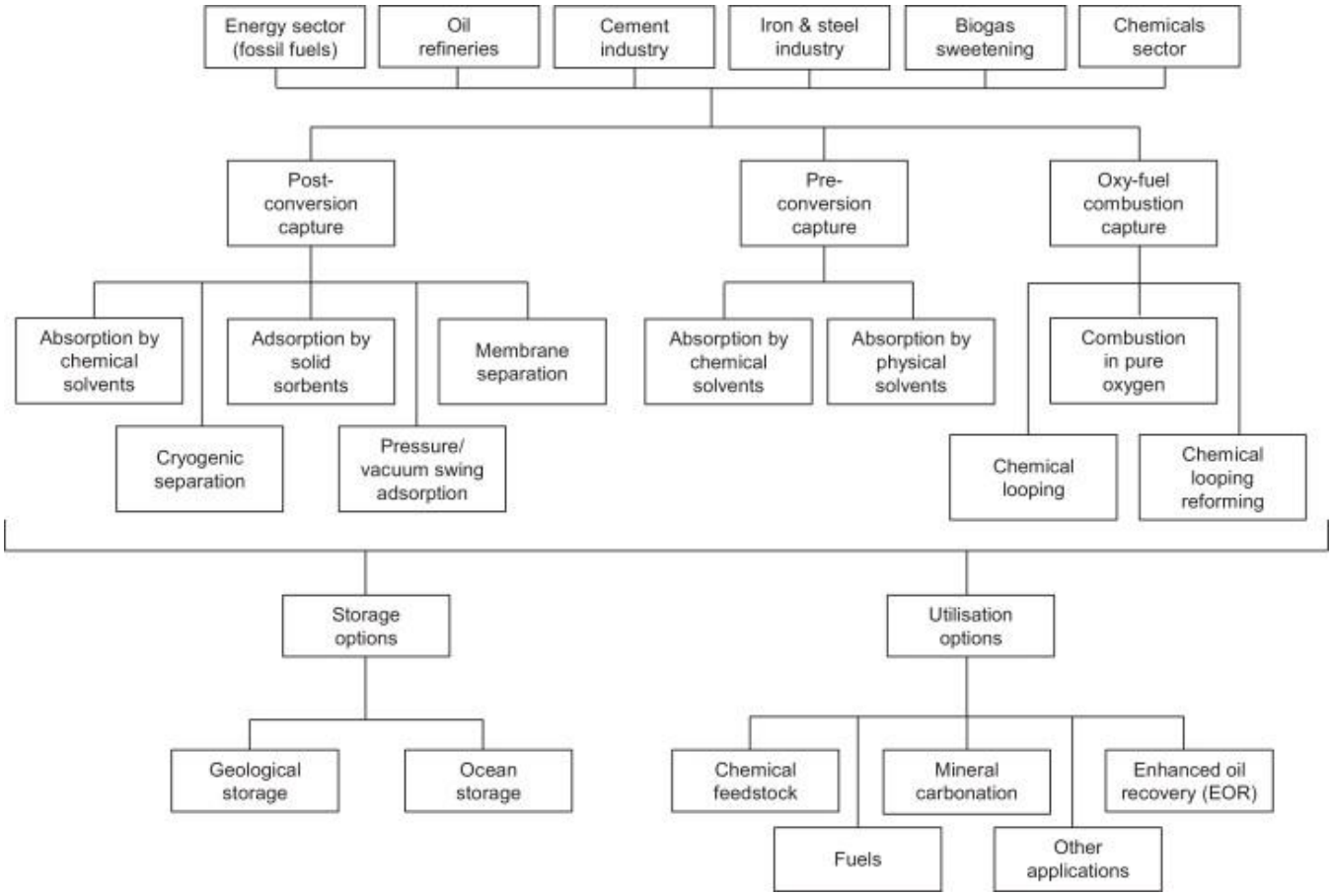

Figure 3 : Overview of carbon capture and storage or utilization [13]

1.2.2.1 Capture

Two main types of capture are possible: post conversion capture and pre-conversion capture (
Figure 4). For each type there is a variety of technologies. This allows the capture method to be adapted to the characteristics of the source.

Post conversion capture is a separation with the effluents carried out after the conversion of the carbon source into CO_2. Pre-conversion capture is defined as the capture of CO_2 as an undesired co-product or reaction intermediate during the process or also in the case of pre-combustion capture. [7]

In both cases different technologies can be used. Among these we can mention membrane separation [14], cryogenic separation [15] but the most widely used are being adsorption and absorption. Absorption in liquid solvents [16] is a widely used method but with disadvantages. Indeed, the used solvents are toxic and induce a high energy consumption by their renewal. Adsorption on solids is therefore a more interesting alternative. The solid in question must have a high selectivity, thermal stability and CO_2 adsorption capacity. Basic zeolites, carbon-based materials, amine-functionalized materials, basic clays among others are good candidates. Once the CO_2 is captured on these materials, a thermal treatment allows it to be reabsorbed either for storage or for use. [7]

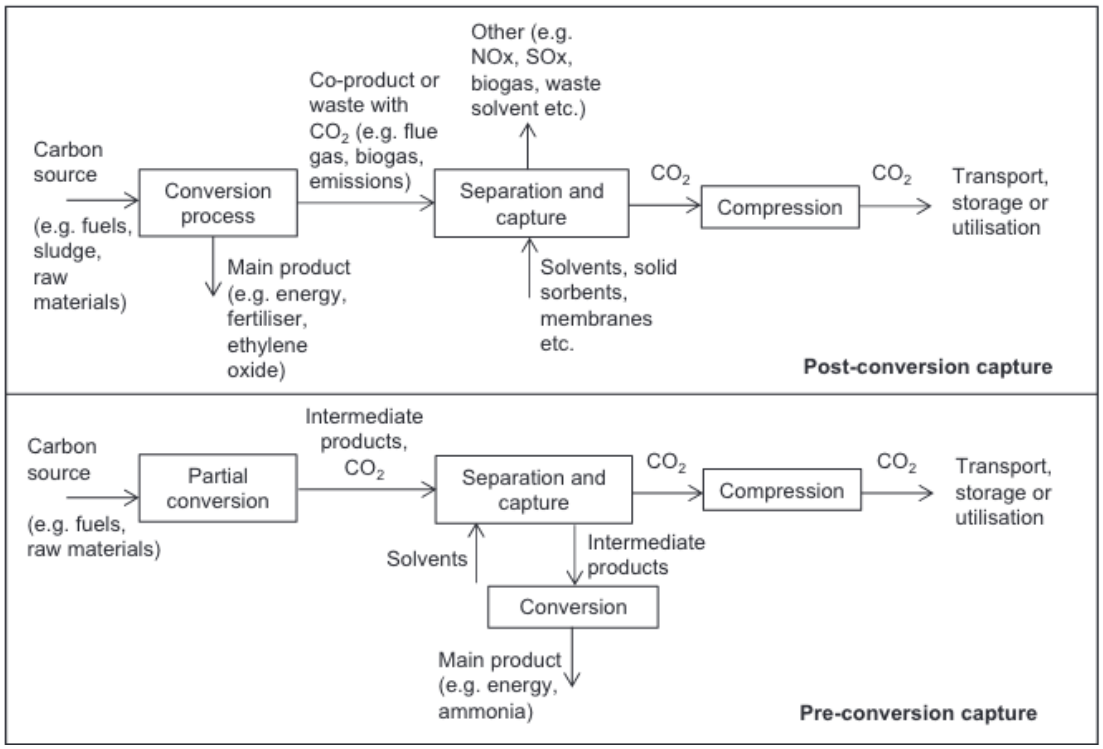

Figure 4 : Carbon capture options explained [13]

1.2.2.2 DAC

This method is based on the adsorption of CO_2. We can distinguish two types of adsorption mechanisms; physical adsorption and chemical adsorption. In the first case, materials such as zeolites, metal organic frameworks (MOFs) and carbon-based materials are used. These are stable and easy to prepare, but do not have excellent adsorption capacity. In the second case, materials such as alkali carbonate-based adsorbents or solid amine-based adsorbents are used. [12]

The main advantage of this type of capture is that it can be carried out anywhere. However, due to the very low concentration of CO_2 in the atmosphere, this technology is very expensive. [12]

1.2.2.3 Storage

In the case of CCS, the captured CO_2 can be stored in different ways (see Figure 5 : Carbon storage options [13]
). First, it can be stored in the ground at a depth of 800 to 100m, this is called geological storage. The CO_2 is then injected into geological formations. Another possibility is storage

in the ocean at great depth. Although this is not an ideal solution (risk of leakage [17]), it remains very interesting because it allows long-term storage of CO_2. [13]

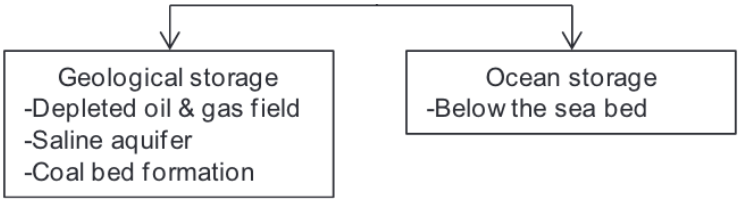

Figure 5 : Carbon storage options [13]

1.2.2.4 Utilization

CCU is gaining increasing interest due to the possibility of producing other interesting molecules (chemicals/fuels) or to sell this pure CO_2 (for example to the food industry) which is particularly interesting in the context of industrial effluent treatment because it allows a revalorization of these unwanted emissions. [18,19]

In the case of conversion, we can distinguish two cases: the production of chemicals and the production of fuels. In the first case CO_2 is used as a precursor for organic compounds in a carboxylation reaction. In the second case it can be used as feedstock to produce fuels[13]. A disadvantage of the latter is that the conversion is energy intensive and requires the use of very selective catalysts. Furthermore, in both cases the CO_2 will quickly return to the atmosphere due to the short life span of these products. The purpose of converting CO_2 into fuel is therefore more to provide a carbon-neutral fuel alternative and a reuse of the emitted CO_2 than to remove CO_2 from the atmosphere.

In order to obtain fuels from CO_2, an hydrogenation reaction can be performed. Different methods exist (see
Figure 6). Examples are the electrochemical approach [20], photocatalytic process [21] or a biocatalytic approach [22]. All with advantages and disadvantages. In this work the focus is on thermal hydrogenation, a process that has the advantage of reaching high yields but requires high temperatures. [18, 23]

Different products can be formed by the thermal hydrogenation of CO_2 depending on the catalyst and the conditions used as shown in
Figure 6. In recent years, our laboratory has been active on the development of heterogeneous catalysts dedicated to the hydrogenation of CO_2 to methane (methanation) [24–26].

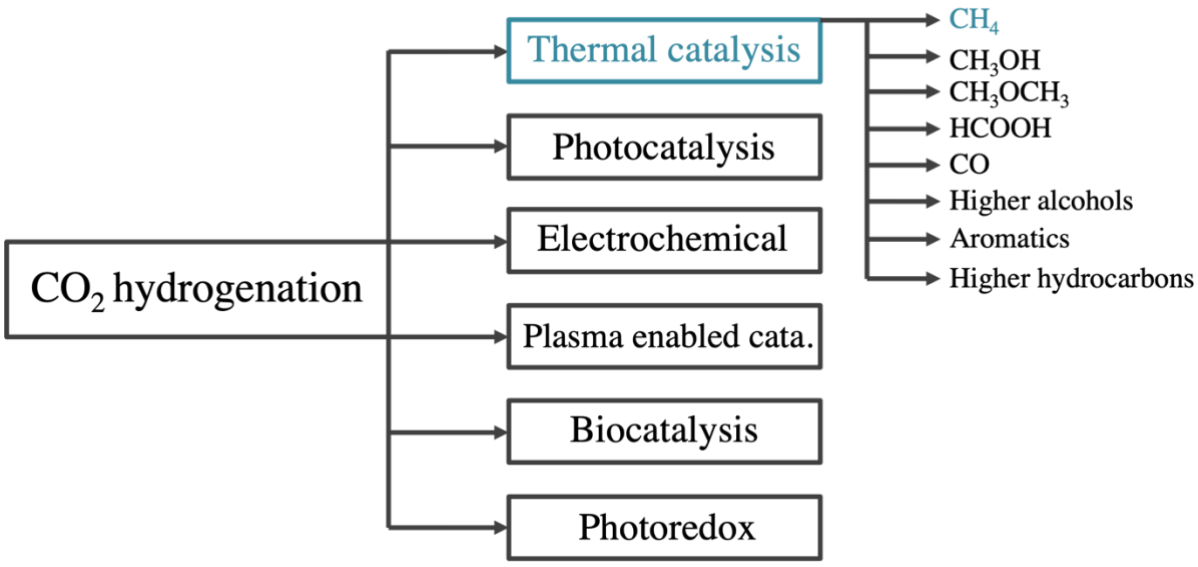

Figure 6 : CO_2 hydrogenation methods and products [18]

1.3 CCU for methane production

1.3.1 Reaction

Two different pathways are possible to produce methane from CO_2. First, the hydrogenation of CO_2 itself via the Sabatier reaction with the use of a catalyst. In this case the reaction is exothermic and occurs as follows [23]:

(1)

$$CO_2 + 4H_2 \leftrightarrow CH_4 + 2H_2O \qquad \Delta H_{298k} = -165.03 \frac{kJ}{mol}$$

The second possible pathway starts with transformation of CO_2 into carbon monoxide via the reverse water gas shift reaction (RWGS). This carbon monoxide can then be transformed into CH_4 via methanation of the carbon monoxide or via the reverse dry reforming reaction with a production of CO_2. The reactions are the following [23] :

First the RWGS reaction:

(2)

$$CO_2 + H_2 \leftrightarrow CO + H_2O \qquad \Delta H_{298k} = 41.17 \frac{kJ}{mol}$$

Followed by either CO methanation:

(3)

$$CO + 3H_2 \leftrightarrow CH_4 + H_2O \qquad \Delta H_{298k} = -206.19 \frac{kJ}{mol}$$

Or by reverse dry reforming reaction (undesired):

(4)

$$2CO + 2H_2 \leftrightarrow CH_4 + CO_2 \qquad \Delta H_{298k} = -247.36 \frac{kJ}{mol}$$

Since the RWGS reaction is endothermic and all reactions leading to methane formation are exothermic, working at high temperatures will thermodynamically favor the formation of carbon monoxide over methane. Moreover, high temperatures favor the appearance of coke and can lead to the degradation of the catalyst. However, a too low temperature would kinetically disadvantage the methanation reaction. It is thus desirable to carry out the reaction at moderate temperature (around 200°C).

This application has a double interest. First, as shown in Figure 7, it provides a carbon-neutral energy source. Indeed, the CO_2 released during the use of methane as an energy source is compensated by the CO_2 captured to synthesize it [23]. However, in order to respect

the carbon neutrality of the process, the choice of the type of hydrogen introduced for the reaction has its importance and will be discussed in 1.3.2.

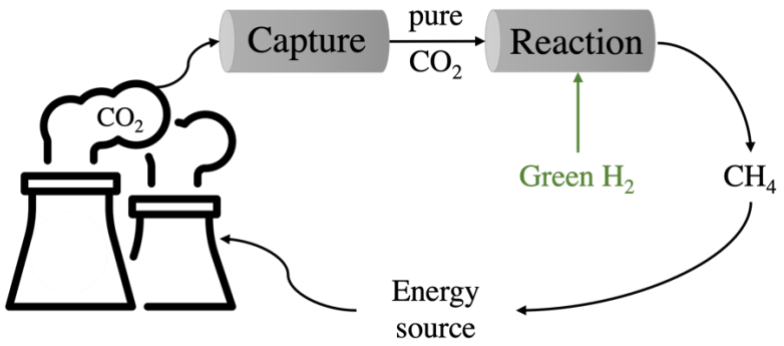

Figure 7 : capture and recycling of CO_2 into CH_4

Then this reaction transforms hydrogen, an energy carrier, into methane. Hydrogen being explosive, it is not easy and safe to transport it, which is less of a problem with methane. This reaction therefore allows the energy carried by the hydrogen to be used in another, safer form.

As mentioned, a catalyst must be used during this methanation reaction. Metals used as catalyst are expensive and can be quite sensitive to degradation. In the case of this application the feed stream is very diluted in CO_2 and other molecules are present (industrial effluents for example). To avoid any degradation of the catalyst, it is preferable to work with pure CO_2. Thus, a capture of the CO_2 before the reaction is necessary. There are different ways to combine this capture step with the catalytic step as will be discussed in 1.3.3. [7]

1.3.2 Hydrogen source

As explained the choice of the type of hydrogen introduced for the reaction will impact the carbon balance of the overall process. Indeed, there are different ways to synthesize hydrogen leading or not to CO_2 emissions. Among the different methods the most used is the one based on methane reforming. It consists of two steps; the vaporeforming and the water-gas shift reaction whose equations are respectively the followings : [18]

(5)

$$CH_4 + H_2O \leftrightarrow 3\,H_2 + CO$$

(6)

$$CO + H_2O \leftrightarrow H_2 + CO_2$$

As this process produces CO_2, the use of such a type of hydrogen ("grey hydrogen ") in the case of CO_2 methanation would lead to a non-zero carbon balance. A possible alternative is

then the use of green hydrogen. The latter is obtained by electrolysis of water powered by renewable energy. The only by-product is oxygen in that second case. Figure 8 summarizes these two different processes. [18]

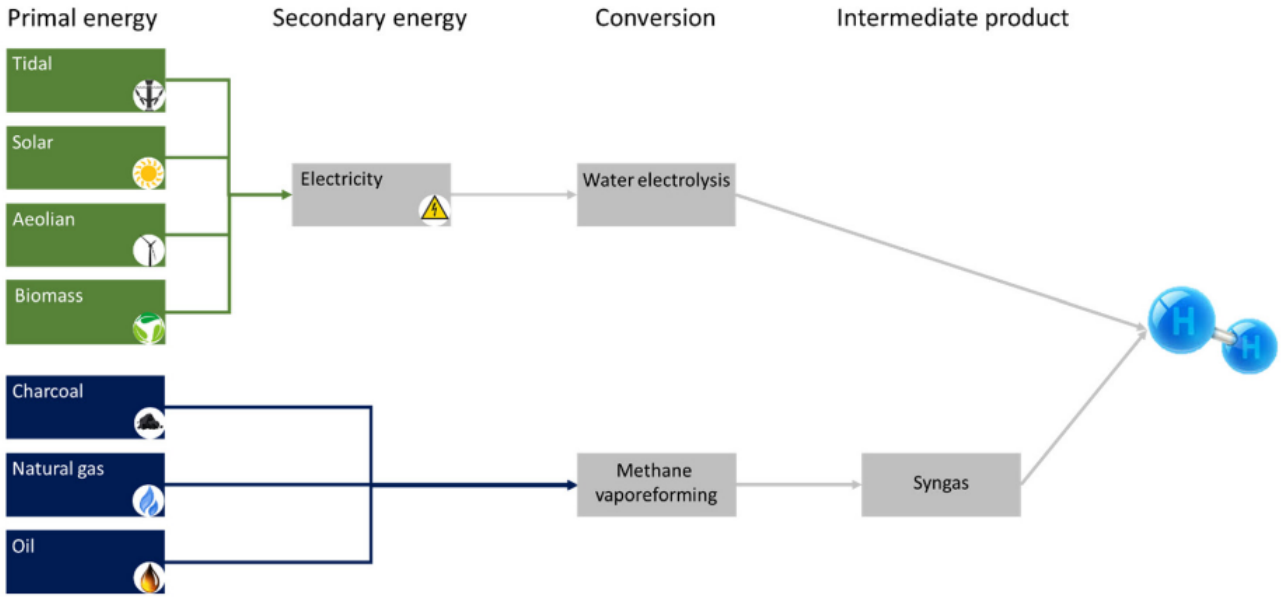

Figure 8 : Pathways for hydrogen synthesis [18]

1.3.3 Combining CO_2 capture and methanation, possibilities

As previously discussed, processed CO_2 effluents are dilute and complex. To avoid catalyst damage, a fairly pure CO_2 stream is required. Since purification processes are expensive, it is worth considering combined processes that allow working directly with the untreated effluent. Different ways to combine capture and methanation steps can be envisaged. The three main ones will be described here.

In a first case the two steps can be carried out in two different units (Figure 9a). The complex effluent passes initially by the unit of adsorption where a solid adsorbent is. A gas flow without CO_2 is then released. When the adsorbent is saturated, the temperature can be increased in order to desorb the pure CO_2. This gas is then led to the catalytic unit where the methanation reaction takes place on the catalyst in the presence of a hydrogen flow.[7]

A second possibility is to work in a single unit with two separate solids for adsorption and reaction (Figure 9b). These solids are either mixed with each other or separated. In this case the gas is always in contact with both types of solids. Depending on the applied conditions (temperature and type of gas flow) one or the other step will take place.[7]

Finally, a single solid combining both carbon capture sites and catalytic sites dispersed on a support can be used in a fixed bed (Figure 9c). This is referred to as a dual function material (DFM). The process proceeds in a similar way to the previous case. [7]

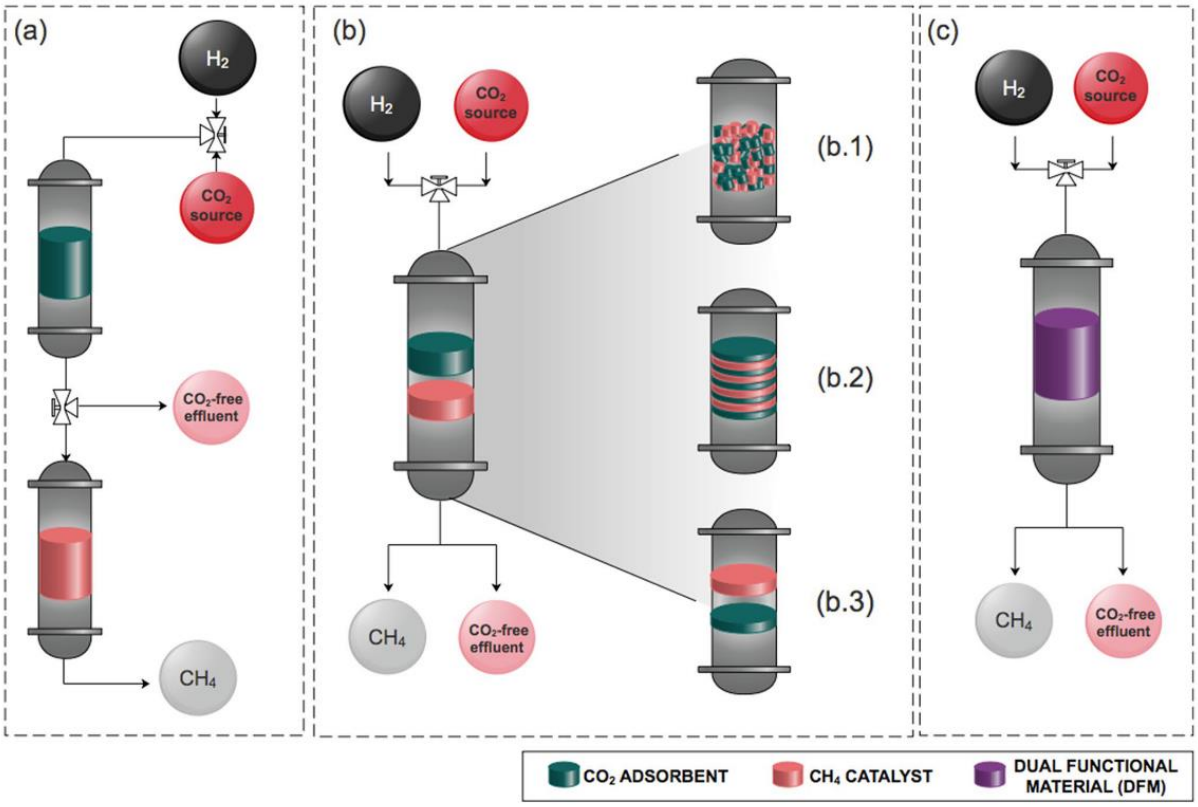

Figure 9 : Different solutions to combine CO_2 capture and methanation [7]

The main advantage of the first case compared to the others is that the separation of the two processes allows to optimize them separately. However, working with two reactors requires more investment. The difference between the second case and the use of a DFM is mainly the possibility or not to optimize the two types of sites used separately. Indeed, in the case of DFM the two types of sites are on a single material it is thus a question of finding a compromise between optimization of the capture and optimization of the methane synthesis during the synthesis. However, DFMs are expected to offer interesting advantages. The proximity between the capture and methanation sites on the DFM allows the process integration at particle scale with lower mass and heat transfer resistances an interaction between them which may results in better performances. [7,27]

1.4 DFM as a solution

As explained the use of DFMs is an interesting solution allowing the combination in one solid of CO_2 capture and methanation. However, it remains quite challenging to optimize these two aspects at the same time. In order to obtain the best possible performance, the choice of basic and catalytic sites plays an important role.

1.4.1 Capture sites

The species used for the capture must feature abundant surface basic sites in order to interact with CO_2. However, this interaction must be neither too weak nor too strong. Indeed, in case of too weak interaction the CO_2 would be easily carried away with the gas flow and thus too little CO_2 would be captured and available to react. In the case of a too strong interaction the captured CO_2 would only be partially released for the reaction, making the process less efficient.

Alkalines and alkaline earths are good candidates for CO_2 capture. The use of lithium (Li), sodium (Na), potassium (K), magnesium (Mg), calcium (Ca) and baryum (Ba) oxides in combination with ruthenium supported on alumina has been tested by the Porta group [28]. Figure 10 shows the CO_2 TPD results for these different species. The vertical axis shows the amount of CO_2 desorbed while the horizontal axis shows the temperature. The more CO_2 is desorbed at high temperature, the more it was strongly bound to the material and therefore the stronger the solicited basic sites are. As observed in Figure 10, Ca, Ba and K form thermally stable carbonates. Thus, CO_2 is less accessible for the reaction in those cases. For Mg and Li, on the other hand, peaks are observed at low temperatures and corresponding to relatively low quantities of CO_2. Na oxide is the most optimal candidate as it adsorbs CO_2 with an intermediate strength which allows for both high capture and easy release during reaction. It will be used in this work and will be present on the DFM as Na_2O. [28]

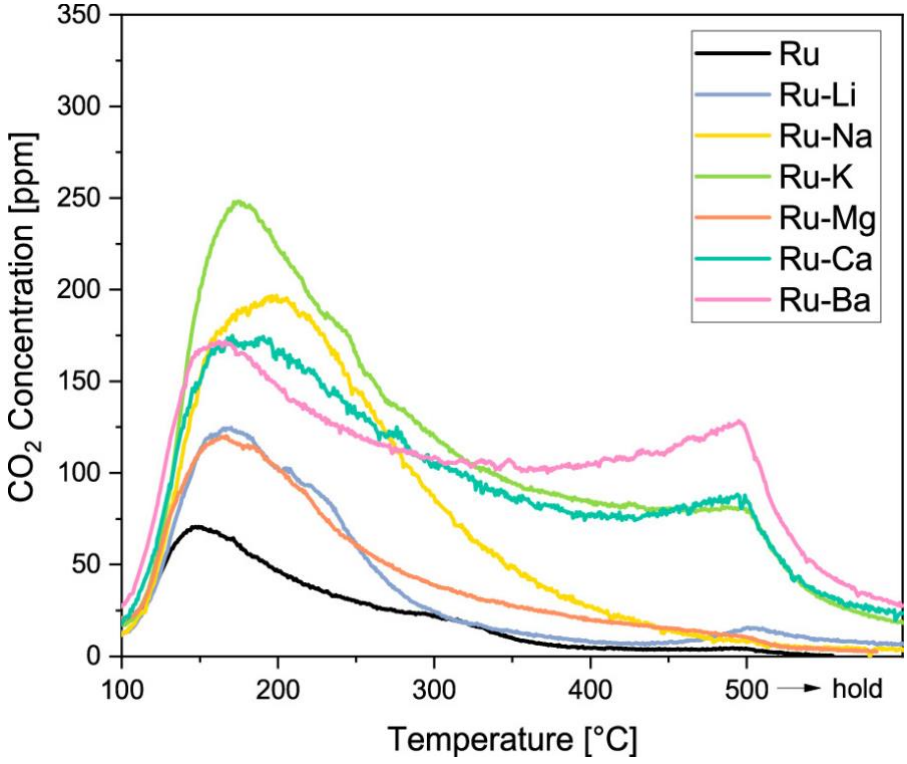

Figure 10 : CO_2 adsorption capacities for different species [28]

1.4.2 Catalytic sites

Among the main active metals for the thermal catalysis of CO_2 methanation one can distinguish two groups: noble metals and non-noble metals. The noble metals include ruthenium (Ru), rhodium (Rh), palladium (Pd) and platinum (Pt). While the non-noble metals include nickel (Ni) and cobalt (Co). Noble metals have the advantage of having a great capacity to dissociate hydrogen. Ru and Rh demonstrate good activity and stability. The disadvantage is that they are quite expensive. The non-noble metals are less expensive and abundant. However, Ni is easily deactivated by sintering despite a good activity. The activity and selectivity of the mentioned metals have been studied in the literature and are listed in Table 1. Nickel and ruthenium are the two most studied metals in the literature for this application. Indeed, we observe a very good activity for ruthenium but a rather bad selectivity in comparison with the other metals. However, in this work the reaction temperature used will be 200°C. Working at moderate temperature with ruthenium favors the formation of methane over carbon monoxide (discussed in 1.3.1 Reaction), enabling high selectivity to be achieved. Ni shows a fairly good activity and selectivity but another problem with this metal is the need to work at high temperature, which is less interesting from an energy point of view. Ru is therefore the metal that will be used in this work. It should be noted that after impregnation, Ru will be present in oxide form (RuO_2) on the DFM, and a reduction step will be necessary to obtain the metallic and therefore active form. [23,29]

Table 1 : Relative activity and selective for different active phases for CO_2 methanation [23]

	Lowest					Highest
Activity	Pd	Pt	Co	Ni	Rh	Ru
Selectivity	Ru	Co	Rh	Ni	Pt	Pd

1.4.3 Reaction mechanism

As explained in 1.3.3, a diluted CO_2 stream is first fed in the reactor, on the DFM. The capture is then mainly carried out on the basic sites where CO_2 will form carbonates. However, CO_2 will also interact with Ru and the alumina support. Once the DFM is saturated with CO_2 the hydrogen flow can be applied to perform the methanation reaction, first with the CO_2 adsorbed on catalytic sites. The injection of hydrogen will then promote a spillover of the carbonate species from the basic sites to the catalytic sites with the formation of formate intermediates, thanks to the energy released by the reaction. The hydrogen also dissociates into hydrides at the catalytic site. The reaction can thus take place between the formates and the hydrides present on the surface of the Ru sites, resulting in the formation of methane. Figure 11 summarizes this process. [30,31]

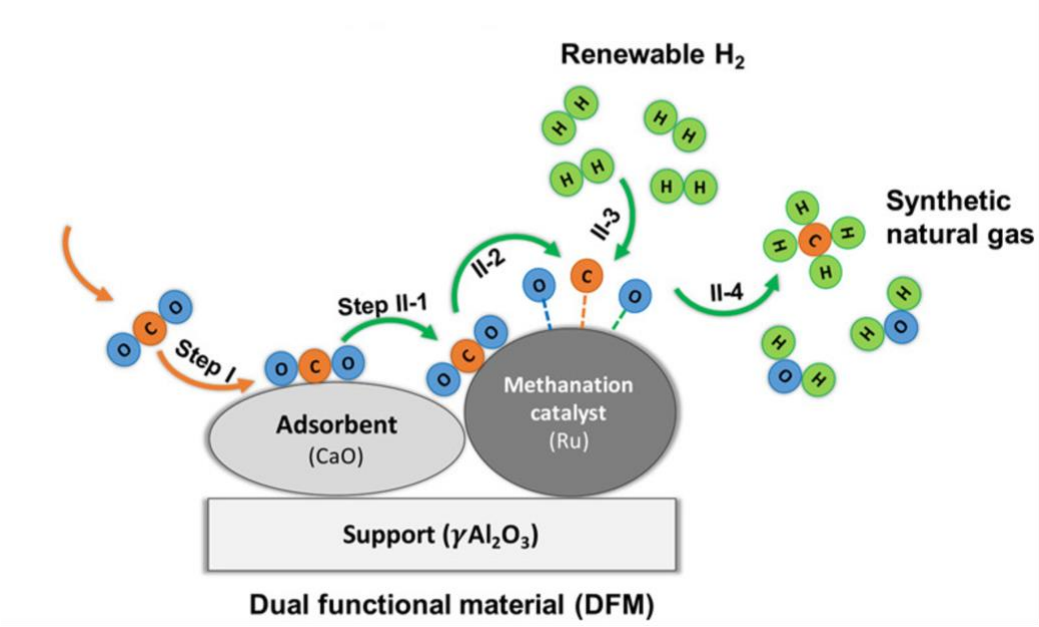

Figure 11 : Reaction mechanism on DFM, adapted from [30]

Given the close interaction between the two types of sites during the reaction, the ratio between basic and catalytic sites is of great importance. Indeed, it is desirable to have a lot of basic sites to capture a maximum of CO_2 which can then react during the methanation step. However, if there are too few catalytic sites compared to the basic sites, the energy

released by the methanation will not be sufficient to release enough of the CO_2 captured on the basic sites.[7]

In the literature, 6% Na_2O – 5% Ru has shown great results. However, the interaction between those sites being quite complex this ratio can still be improved.

2 Objectives and strategies

The objective of this study is to optimize the use of DFM for CO_2 methanation. To do so, two approaches are used: optimization of the synthesis process and optimization of the formulation.

For the first approach, the samples studied were DFMs synthesized by impregnation with 6% Na_2O calcined at 400°C, followed by impregnation with 5% RuO_2 calcined at 200, 250, 300 and 450°C respectively on gamma alumina. It is believed that calcination temperature plays a role on dispersion and particle size which can impact performance of the catalyst [32,33]. The objective will be to observe the changes provoked by the different calcination temperatures and how it impacts catalytic performances. Once an optimum calcination temperature has been determined, the second approach is studied. In this case, the samples are DFMs resulting from impregnation with 6% Na_2O at 400°C, followed by impregnation with 1, 2, 4 and 5% RuO_2 respectively on gamma alumina. As explained in 1.4.3, ratio between basic sites and catalytic sites plays a major role. The objective is to optimize this ratio to obtain optimal catalytic performances.

In order to characterize the different catalysts and to evaluate their performance various techniques were used; XRD, nitrogen physisorption, CO_2 TPD, DRIFTS and finally catalytic tests. XRD provides information on the structure and phase identification of crystalline materials. Physisorption allows to characterize the texture of the material. TPD gives information on the basicity of the CO_2 adsorption sites. The DRIFTS allows observing the species formed on the surface of the material during the course of the reaction. Finally, the catalytic testing allows observing and quantifying the capture of CO_2 and the production of methane

3 Materials and methods

3.1 Materials

Gamma alumina (γ-Al_2O_3) was used as support for the DFM, supplied by Alfa Aesar.

The precursor used for Na_2O basic sites was sodium carbonate (Na_2CO_3; ≥ 99.5%), supplied by Roth.

The precursor for Ru catalytic sites was Ruthenium(III) nitrosylnitrate ($Ru(NO)(NO_3)_3$; Ru ≥ 31.3%) from Alfa Aesar.

3.2 Methods

3.2.1 DFM synthesis

3.2.1.1 General method

The DFM is synthesized via two successive wet impregnations on the alumina support. This method is used to fix the different sites on the surface of the support by putting them in solution and evaporating the water to obtain a powder.

The impregnation of the basic sites is done first. A solution of sodium carbonate (Na_2CO_3) is prepared, alumina (γ-Al_2O_3) is then added. The resulting solution is mixed with a magnetic stirrer at 500 rpm for 30min. Then the water is evaporated first in a rotavapor at 60°C for about 1 hour (until a solid residue is obtained) and then in an oven at 120°C for 2 hours. The obtained powder is finally calcined at 400°C for 4 hours with a ramping of 10°C/min. Impregnation of the catalytic sites is then performed. The same process is used here with a ruthenium precursor solution ($Ru(NO)(NO_3)_{3)}$ to which the product of the first impregnation is added. The calcination temperature is lower in this case. The temperature used in the previous thesis is 250°C. In this work, different calcination temperatures have been tested. Figure 12 illustrates the DFM preparation.

The reference percentages of basic and catalytic sites are respectively 6% and 5%. These have been chosen from previous works. Different percentages of catalytic sites were then tested in this work.

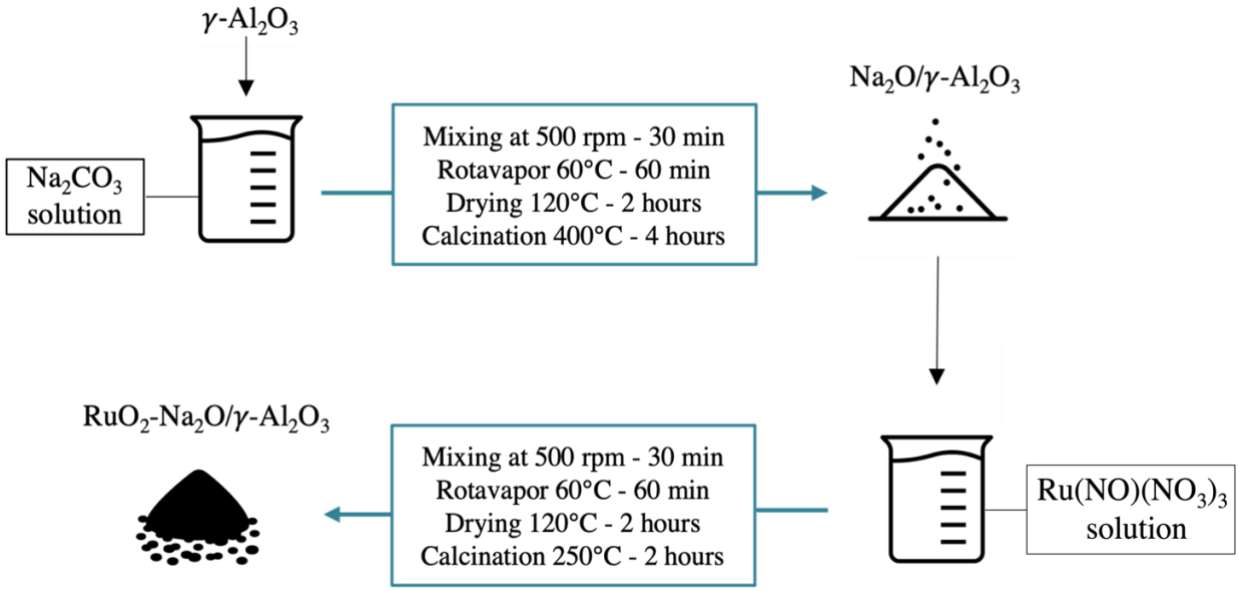

Figure 12 : DFM preparation method

3.2.1.2 Different calcination temperatures for second impregnation

The impact of different calcination temperatures for the ruthenium impregnation step on the performance and characteristics of the catalyst was tested. This was done for catalysts with a composition of 5 wt% Ru and 6 wt% Na_2O. For all samples the impregnation of the basic sites was done in one batch and then separated into different batch for the second impregnation. The synthesis process is identical to the one described in *General method* except for the second impregnation temperatures. The tested temperatures are 200°C, 250°C, 350°C, 450°C. A lower ramping rate of 5°C/min was used in order to avoid overshooting, especially for calcination à 200 and 250°C. The table below summarizes the characteristics and the names of the different catalysts.

Table 2 : Catalysts information for different calcination temperatures

Catalyst	Ru loading (%)	Na_2O loading (%)	1st calcination temperature (°C)	2nd calcination temperature (°C)
Ru5-200	5	6	400	200
Ru5-250	5	6	400	250
Ru5-350	5	6	400	350
Ru5-450	5	6	400	450

3.2.1.3 Different Ru loadings

After the calcination temperatures it was the loading of ruthenium that was varied. After analysis of the results for the different calcination temperatures (discussed in Results) it was decided to work with a temperature of 450°C for all samples. The procedure is identical to the one described in *General method* but with different loading. The loadings tested were 1%, 2%, 4% and 5% Ru, Table 3 shows the information for each sample. The sample with 5% has not been resynthesized. For the other samples a mass of 2g of the product of the first impregnation was used each time. The mass of ruthenium precursor used each time is presented in Table 4.

Table 3 : Catalysts information for different Ru loadings

Catalyst	Ru loading (%)	Na_2O loading (%)	1st calcination temperature (°C)	2nd calcination temperature (°C)
Ru1-450	1	6	400	450
Ru2-450	2	6	400	450
Ru4-450	4	6	400	450
Ru5-450	5	6	400	450

Table 4 : Ru precursor masses for different Ru loadings

Catalyst	Ru loading (%)	Na_2O/Al_2O_3 mass (g)	Ru precursor mass (g)
Ru1-450	1	2	0,063
Ru2-450	2	2	0,128
Ru4-450	4	2	0,261

3.2.2 Characterization techniques

3.2.2.1 X-ray diffraction (XRD)

XRD is used to identify the crystalline phases present in the DFM. The diffractograms are obtained with the Bruker D8 Advance system. The samples undergo Cu K-α radiation with a wavelength of 1.5419 Å, an angle 2θ between 5° and 80° and a step size of 0.02° and 20s/step. The data are analyzed with the DIFFRAC.EVA program and with the PDF2-2004 database.

From the obtained peaks, the size of the crystal sites can be calculated using the Scherrer equation. This equation is the following:

(7)

$$d_{p,XRD} = \frac{K.\lambda}{\beta.\cos(\theta)}$$

With

$d_{p,XRD}$ = average crystal size (nm)

K = shape factor (0.9 in this work)

λ = X-ray wavelength (which is 1.5419 Å for Cu K-α radiation)

β = broadening of the peak at half maximum intensity

θ = diffraction peak angle

3.2.2.2 N_2 physisorption

This method allows to characterize the texture of the sample, more precisely the specific surface (by BET method) and the porosity by using isotherms of adsorption-desorption of liquid nitrogen on the sample.

Between 100 and 150 mg of sample are taken. Before the measurement the sample must be degassed for several hours at 170°C until a pressure < 100 mTorr is obtained. This step is performed with a VaxPrep 061 from Micromimetics.

The measurement is done in a liquid nitrogen bath (temperature of 77K). The isotherms are obtained using a Tristar from Micromimetics.

3.2.2.3 CO_2 temperature programmed desorption (CO_2 TPD)

This method allows to measure the basic properties of the material. The analysis is performed with a Hiden CATLAB-PCS combined with a Hiden QGA spectrometer analyzing the outgoing gases.

The temperature and gas flow program used is the following:

- Reduction of the sample at 200°C for 90 min (including 30 min of heating) under a 5% H_2:Ar flow (30ml/min)
- Cooling from 200°C to 50°C under a 100% Ar flow (30ml/min)
- CO_2 adsorption at 60°C until saturation under 15% CO_2:Ar (30ml/min). The temperature is maintained at 60°C for 3 hours.
- CO_2 desorption at a temperature ranging from 50°C to 700°C, with a ramp of 10°C/min.

3.2.2.4 In situ Diffuse Reflectance Infrared Fourier Transform Spectroscopy (DRIFTS)

This qualitative method allows the chemical analysis of the surface of materials during a reaction. It will therefore allow to observe the intermediate chemical bonds created or consumed on the surface of the DFM during each step of the catalytic cycle; CO_2 adsorption, He flushing and methanation. The spectrometer used for this measurement is the Bruker Equinox 55 FT-IR which works in a wavelength range between 4000 and 800 cm^{-1} and at a resolution of 4cm^{-1}. The OPUS software gives a spectrum every minute from which the background noise is subtracted. This background corresponds to the spectrum obtained for the material under 100% He atmosphere.

Prior to the measurement, the samples are diluted in KBr at a rate of 90% KBR for 10% DFM. This manipulation makes it possible to increase the signal of the DFM which is dark because of the reflectivity of KBr. It is also necessary to carry out a reduction beforehand during 1h at 200°C (as made at the time of the cyclic tests)

3.2.3 Catalytic testing

The catalytic tests are performed on a fixed bed in a stainless-steel reactor (outside diameter = 8mm, bottom diameter = 6mm, length = 280mm) at a constant temperature of 200°C. This optimal temperature was determined in the previous thesis by an optimization test.

The CO_2 capture and methanation steps are performed separately, with a helium flush between each step. The gases leaving the reactor are continuously measured by mass spectroscopy (MS). The instrument used for this measurement is the Pfeiffer vacuum ThermoStar which allows a qualitative and quantitative measurement.

Before being installed in the reactor the catalyst is pelletized and then crushed and sieved to retain only the particles with a size ranging from 100 to 315 um. Once in the reactor and before starting the capture and methanation steps, the catalyst must be reduced under a hydrogen flow of 30ml/min at 200°C for one hour. The amount of hydrogen used is in

excess to ensure that all the DFM is reduced and therefore usable for the reaction that follows.

Once these preparation steps are completed, the cycles can be started. They proceed as follows:

- Helium flush for 30 min (30ml/min)
- 30 min CO_2 capture (CO_2 flow at 6ml/min in helium flow at 24ml/min)
- 35 min helium flush (30ml/min)
- 1 hour methanation of the captured CO_2 (hydrogen flow at 30ml/min)

This cycle is repeated 3 times per catalytic test.

This test quantifies both the amount of CO_2 captured and the amount of methane produced using the data obtained by the MS. For methane this calculation is quite simple. Once the baseline is removed, the amount can be calculated from the area under the methane production signal curve as shown in Figure 13. Concerning the amount of CO_2, it is a bit more complex. Indeed, among the CO_2 adsorbed during the capture step, a weaker part will be desorbed during the next flush step. The CO_2 available for the reaction will be the CO_2 adsorbed during the capture step minus the one desorbed during the flush step. Also, we observe a desorption of CO_2 during the reaction step.

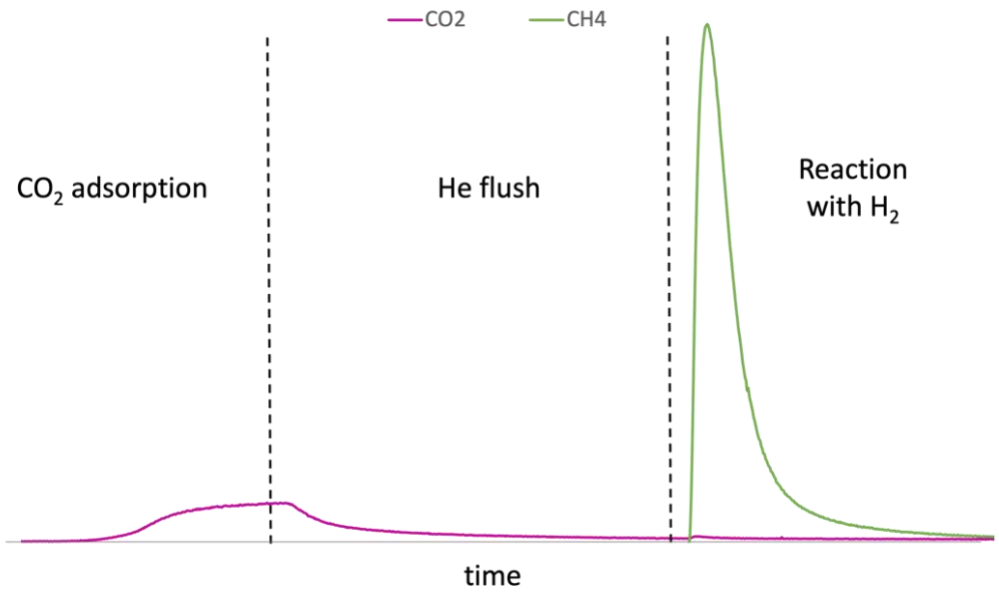

Figure 13 : Catalytic testing profile

4 Results

This section presents the results of the various analyses carried out for the two DFM optimization approaches, as well as an analysis of these results. Optimization through the choice of calcination temperature for ruthenium impregnation was carried out first. This was to ensure that we were working at the optimum calcination temperature for optimization via ruthenium loading.

4.1 Optimizing DFM synthesis: Impact of calcination temperature

The preparation involves the impregnation of Na_2O and a subsequent calcination. Then, the impregnation of RuO_2 and a final calcination. Considering that this last step can have an impact on the properties of dispersion and particle size of Ru which might affect performance [32,33], we embark in a systematic study of the impact of the calcination temperature for this second impregnation.

4.1.1 N_2 physisorption

In a first step, N_2 physisorption was performed on 3 samples; gamma alumina which is the support, Na_2O/Al_2O_3 which is the product of the first impregnation and $Ru\text{-}Na_2O/Al_2O_3$ which is the DFM. The isotherms shown in

Figure 14 show a similar shape for these three samples. The isotherms are all of type IV, the materials have mesopores (2-50 nm diameter according to IUPAC). However, we observe a lowering of the isotherms for the products of the first impregnation and the DFM in comparison with the support alone. The DFM whose isotherms are shown here corresponds to the sample calcined at 450°C for the second impregnation.

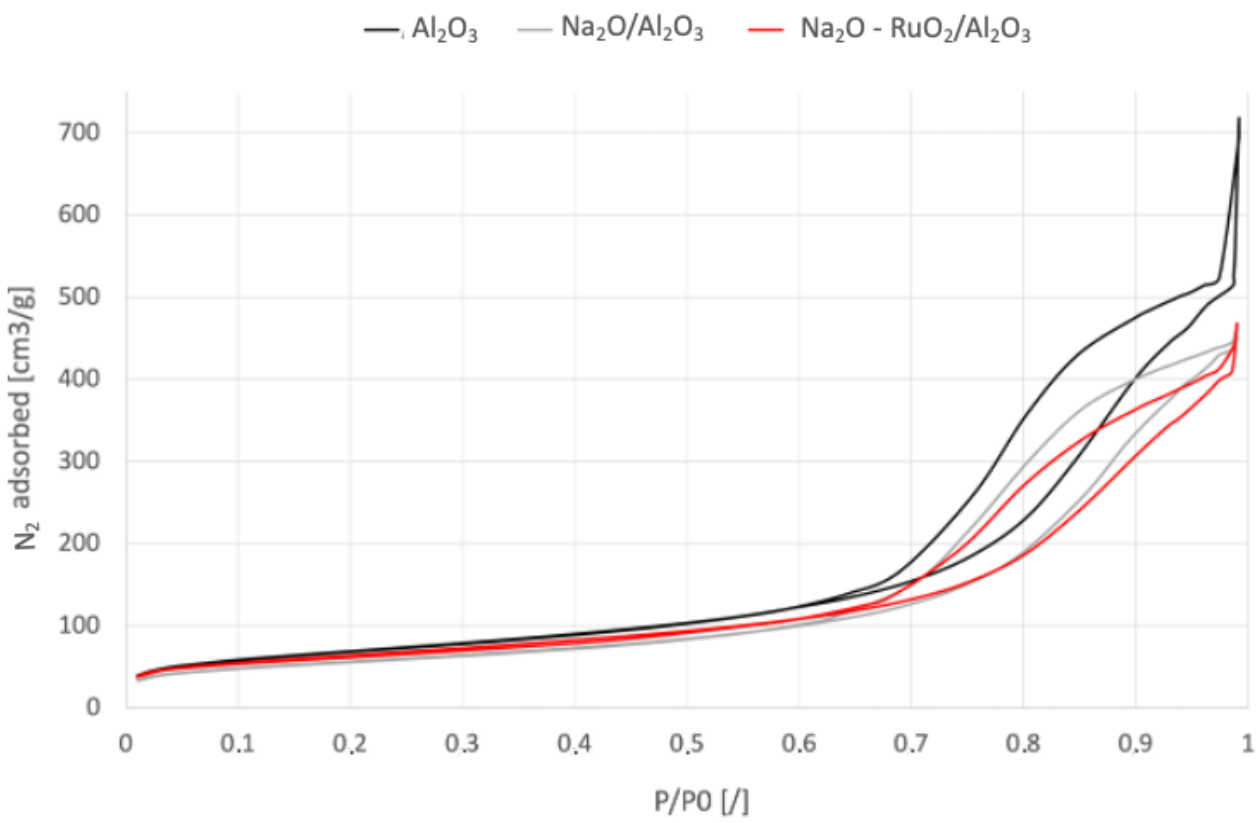

Figure 14: Adsorption isotherms

Considering now the N_2 physisorption on DFM calcined at different temperatures after. Ru impregnation, the isotherms are very similar (Figure 15). Consistently, the BET surfaces as well as the pore volumes of the different samples show similar results as shown in Table 5. It can then be concluded that the calcination temperature for the second impregnation does not impact the textural characteristics of the DFM.

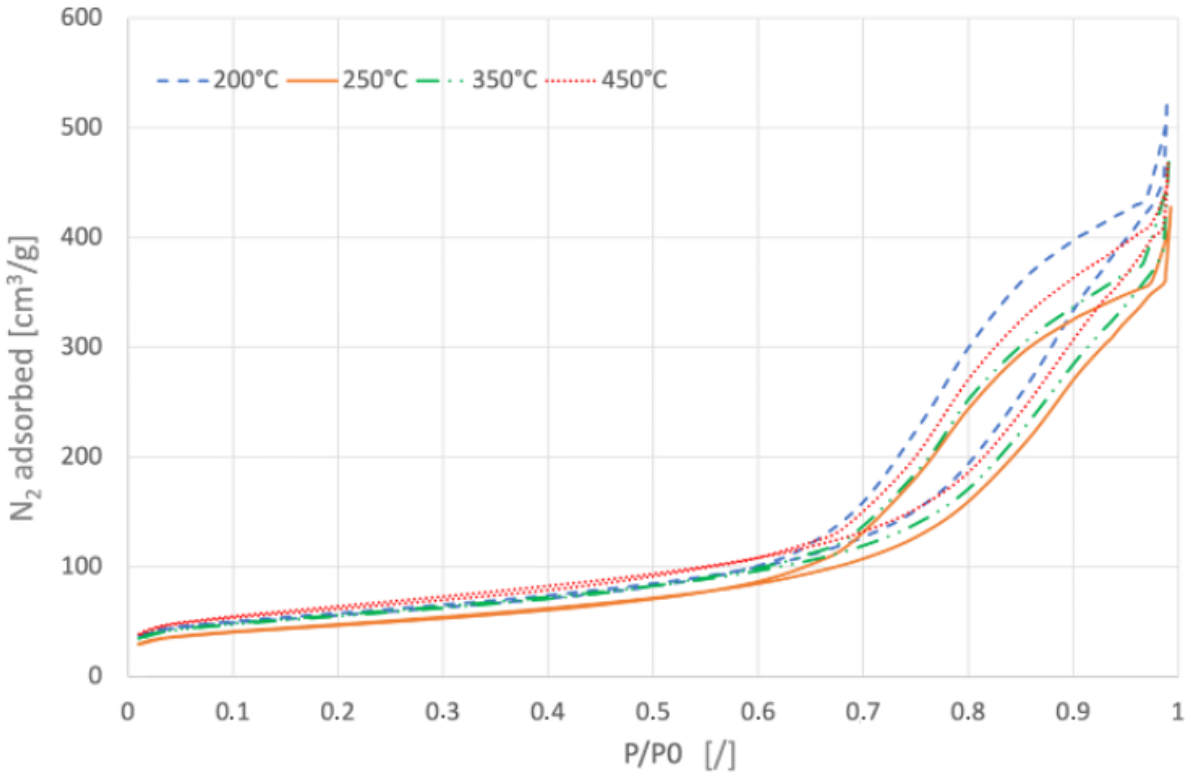

Figure 15 : Adsorption isotherms for different calcination temperatures (5%Ru-6%Na_2O/Al_2O_3)

Table 5 : DFM textural characteristics for different calcination temperatures

	Ru5-200	**Ru5-250**	**Ru5-350**	**Ru5-450**
BET surface area (m^2/g)	200	170	200	230
Pore volume (cm^3/g)	0.70	0.57	0.60	0.64

Regarding now the evolution of the characteristics of structures according to the different stages of the synthesis resumed in Table 6, we can observe here a decrease of BET surface area and pore volume with the addition of basic sites on the support. This shows an occupation of the pores by the basic phase during the first impregnation. On the other hand, the addition of Ru does not modify the texture of the material. Note that in Table 6 for the DFM (RuO_2-Na_2O/Al_2O_3), the BET surface area and the pore volume are both an average of these values for the different calcination temperatures.

Table 6 : Sample textural properties

Sample	**BET surface area (m^2/g)**	**Pore volume (cm^2/g)**
Al_2O_3	250	0.81
Na_2O/Al_2O_3	200	0.69
RuO_2-Na_2O/Al_2O_3 (average)	200	0.63

4.1.2 XRD

In order to identify the different crystalline species present in the DFM, an XRD analysis was performed on the different samples. The obtained diffractograms (Figure 16) allow highlighting the presence of crystalline structures for ruthenium oxide (RuO_2) and for alumina (Al_2O_3). The peaks identified for RuO_2 correspond to 2theta values of 28° (110), 35°(101) and 54° (211) [34,35]. Those for Al_2O_3 correspond to values of 36° (222), 46° (400) and 68° (440) [35,36]. It can be noted that no peaks are observed for the basic sites (Na_2O); this species is amorphous. Also, the peaks observed for ruthenium correspond to the oxide form and not the metallic one. This form being inactive for the catalysis of methanation confirms the necessity of a reduction step of DFM before the reaction. A third crystalline species is noticed at 29°, 39° and 48° [37] for the samples calcined at 200°C and 250°C only. It corresponds to sodium nitrate ($NaNO_3$). The presence of this species was not initially expected and results from the reaction between the basic sites and the RuO_2 precursor ($Ru(NO)(NO_3)_3$) during the second impregnation. It suggests that at 250°C and below, sodium nitrate does not decompose into sodium nitrite. However, the literature suggests that decomposition of this species only begins at around 450°C [38]. We therefore suspect an overshooting issue for the sample calcined at 350°C. The RuO_2 peaks for the sample calcined at 200°C are less sharp than for the other samples. Apart from these two points there is no major difference to be highlighted for different calcination temperatures.

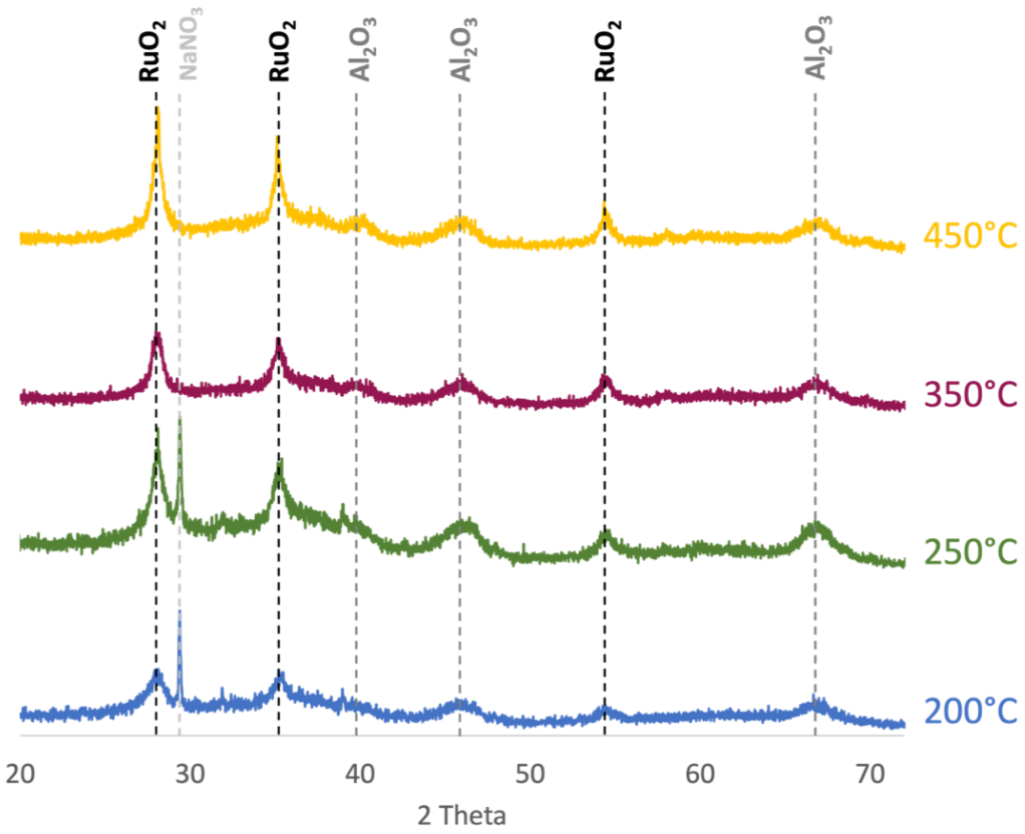

Figure 16 : Diffractograms for DFM calcinated at different temperatures

To confirm this, the size of the crystallites can be determined from the average of (110), (101) and (211) planes of RuO_2 in diffractograms and using the Scherrer equation (7). The results obtained for the different samples are presented in

Table 8. It can be observed that Ru5-200 has the smallest RuO_2 crystallite size and higher calcination temperatures favors the buildup of larger crystallite size. However, no trend can be observed among the catalyst calcined at 250, 350 and 450°C.

Table 7 : Size of RuO_2 crystallite sites for different calcination temperatures

	Ru5-200	Ru5-250	Ru5-350	Ru5-450
(110)	120	180	157	177
(101)	123	172	136	218
(211)	143	210	146	195
Average size (Å)	**129**	**187**	**146**	**197**

XRD was also performed on the spent catalysts (after evaluation of capture and catalytic performance, see 3.2.3 Catalytic testing). The diffractograms are shown in Figure 17. The

major difference with fresh catalysts is the appearance of the peak corresponding to metallic Ru (44°) [34] and the disappearance of those corresponding to Ru in oxide form. Also, the $NaNO_3$ peaks are no longer observed for the samples calcined at 200°C and 250°C. This suggest that under hydrogen $NaNO_3$ can decompose at lower temperature.

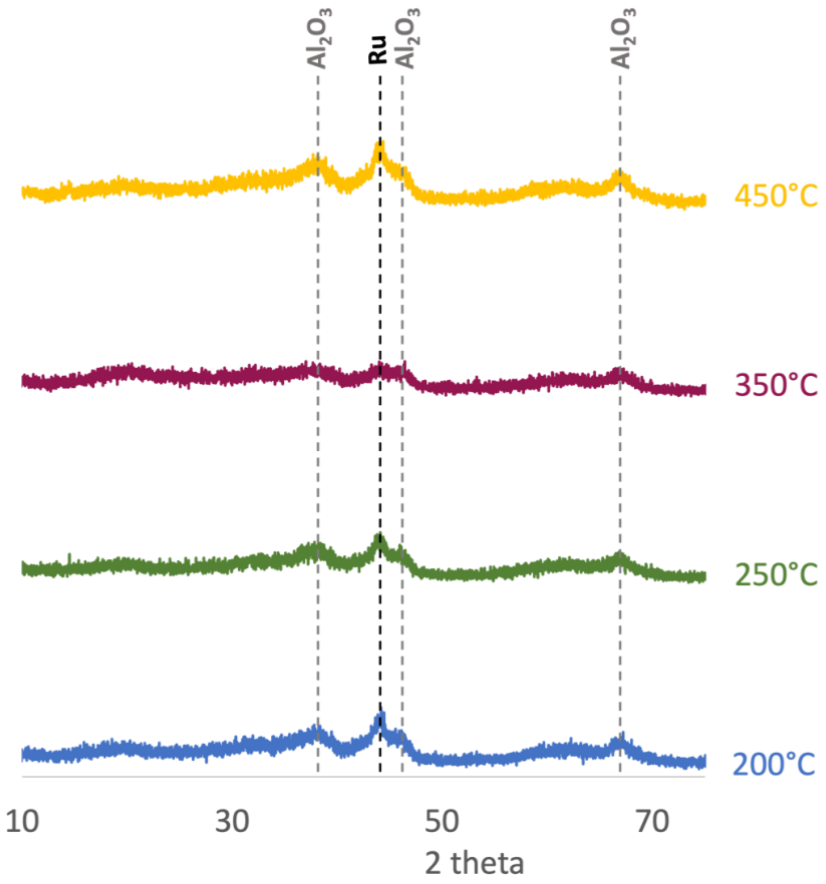

Figure 17 : Diffractograms for spent catalyst for different calcination temperatures

4.1.3 CO_2 TPD

In order to identify the strength of the basic sites present on the DFM, a CO_2 TPD was performed. Depending on the temperature at which the CO_2 is desorbed, three types of adsorption sites can be identified. Below 200°C, the sites can be considered as having a weak interaction with CO_2. From 200 to 400°C these sites have an intermediate interaction. Above 400°C the interaction is strong. [39,40,41]

Figure 18 shows the results for different calcination temperatures. The first observation is that all profiles are similar. They all show two major peaks. The first of weak interaction and the second of medium to strong interaction. There are, however, a few differences. The peak corresponding to sites of medium to strong interaction is slightly shifted towards

higher temperatures for the sample calcined at 450°C. This suggests slightly stronger interaction sites compared with the other samples. The same peak for the sample calcined at 200°C is lower than the others but located at the same temperature. This suggests comparable interaction strength but less CO_2 capture.

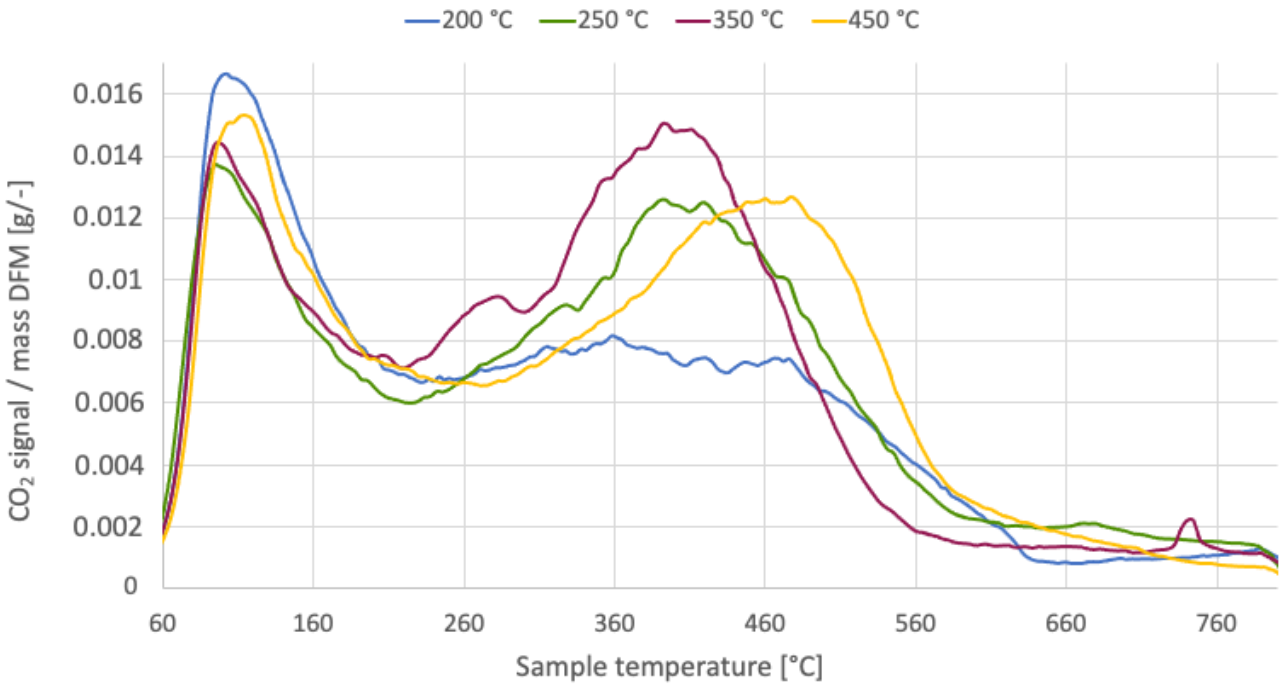

Figure 18 : CO_2 TPD for different calcination temperatures

In order to be able to correctly compare these samples for the reaction carried out, it is necessary to identify the adsorption sites solicited during the reaction. To this end, a CO_2 TPD was carried out on a fresh sample with adsorption at 60°C, as well as on the same sample but with adsorption at 200°C, and on the spent sample for which no adsorption was made before analysis. The analysis of the fresh sample with adsorption at 200°C makes it possible to identify sites that interact too weakly with CO_2 to adsorb it at the reaction temperature (200°C). Analysis of the spent sample allows to identify the CO_2 remaining after reaction, which is linked to sites that are too strong to react.

Figure 19 shows the results of the analysis of these different samples. These results allow identifying the CO_2 released between 200°C and around 350°C as being the one predominantly used in the reaction. This corresponds to medium interaction sites. We can therefore conclude that the reaction conditions (hydrogen injection and heat release by the methanation reaction) favor the desorption of CO_2 bound to stronger sites than when a simple TPD is performed at reaction temperature (200°C).

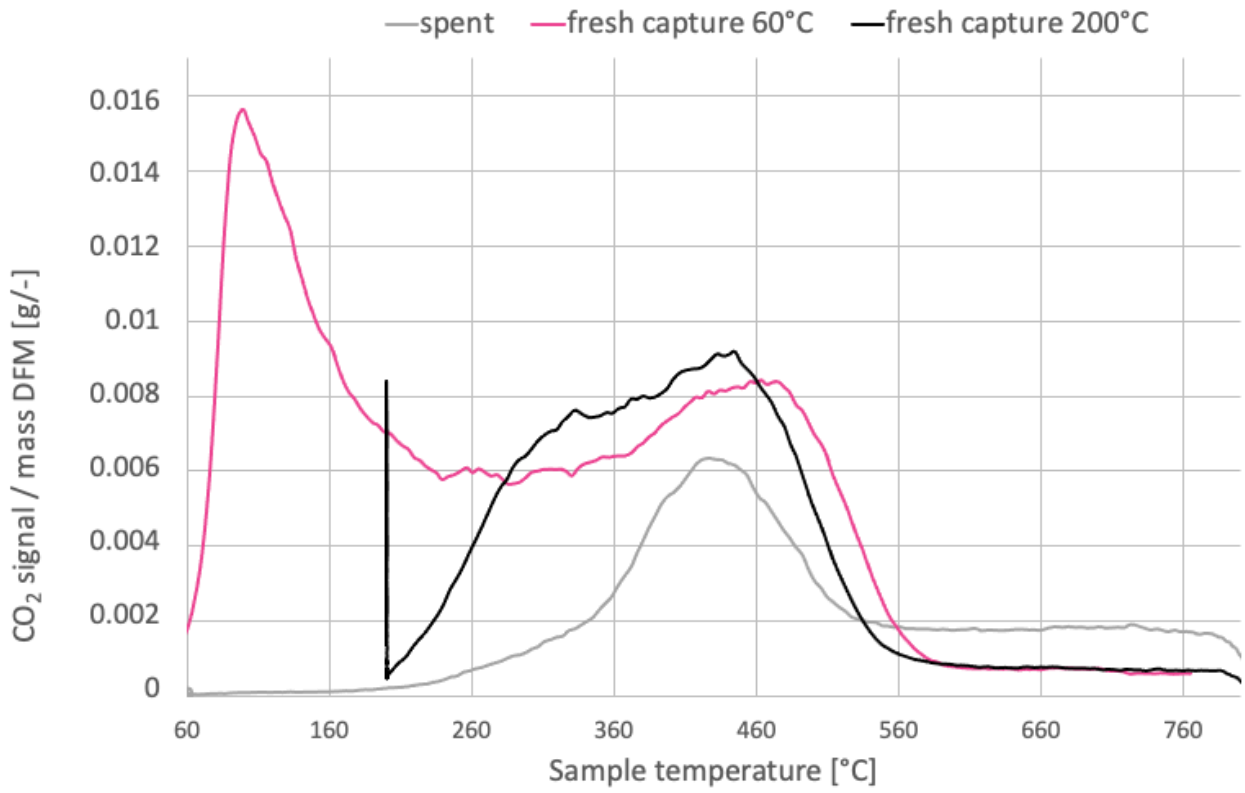

Figure 19 : CO_2 TPD, identification of available CO_2 during reaction

4.1.4 Catalytic testing

The quantities of CO_2 adsorbed as well as the quantities of methane produced for the different DFMs are shown in Table 8. These results are averages of the results for the second and third cycles because these two cycles show consistent results each time. The amount of CO_2 reported here is the amount adsorbed during the capture step minus the amount desorbed during the flush, as explained in 1.2. Slightly better results can be observed for catalysts calcined at higher calcination temperatures although this difference is minor. Conversion rates, calculated as the ratio between the quantity of methane produced and the quantity of CO_2 captured, show fairly constant results. Also, no carbon monoxide production has been observed, the selectivity toward methane is thus 100%. Thus, it can be concluded that the variation of the calcination temperature from 200°C to 450°C for ruthenium impregnation has only a marginal impact on the performance of the DFM.

Table 8 : CO_2 capture and CH_4 production of different catalysts

Catalyst	**CO_2 catpured (moles/kg DFM)**	**Methane produced (moles/kg DFM)**	**Conversion (%)**
Ru5-200	0.18	0.12	66
Ru5-250	0.15	0.11	71
Ru5-350	0.20	0.13	65
Ru5-450	0.21	0.13	62

In order to confirm these results, the methane production profiles can also be used. These profiles represent the helium-normalized methane signal for which the baseline has been adjusted, over a period of 1000 seconds. Indeed, if the peak of the profile arrives faster and the peak is sharper, this corresponds to a faster production of methane, which can be considered as more efficient. These profiles for the studied samples are shown in Figure 20. These are considered for the second reaction cycle. The profiles are globally quite similar. Considering also the results of

Table 8 we can conclude that the sample calcined at 450°C is slightly more efficient. Indeed, it is the one that produces the most methane and the fastest.

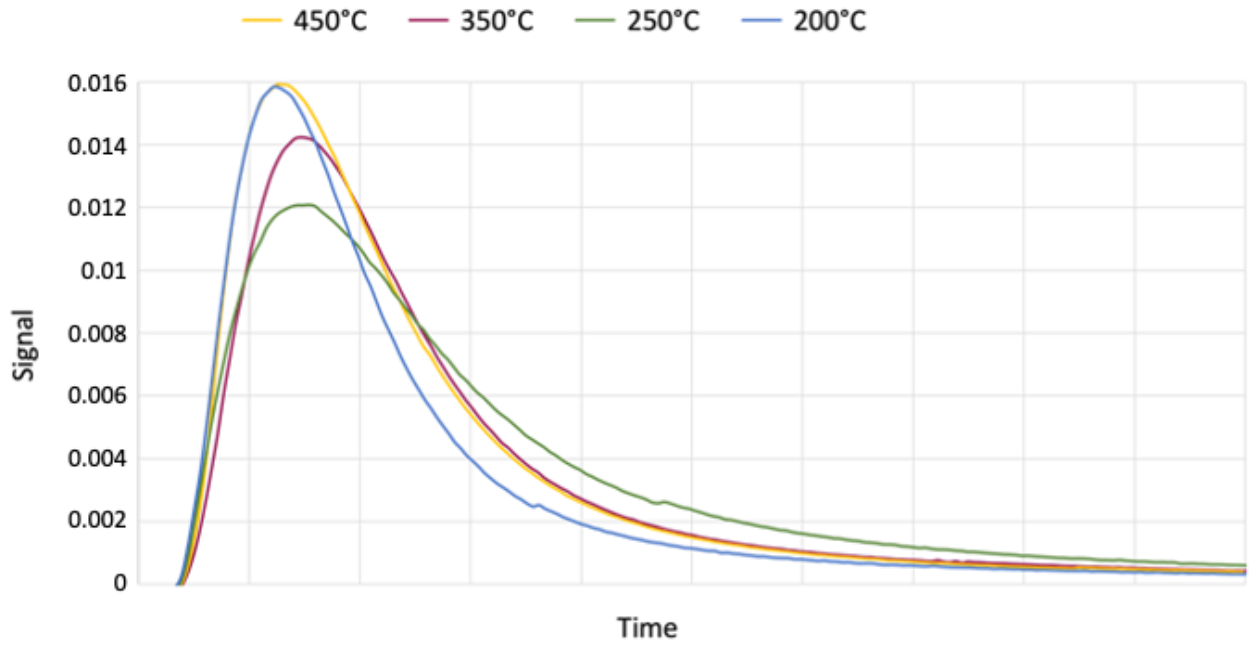

Figure 20 : CH_4 production profile for different calcination temperatures

4.1.5 In situ DRIFTS

In situ DRIFTS measurements allow observing the species that can be formed and transformed at the surface of the material over time. This allows to better understand the

process followed during the reaction. This measurement has been performed here for the Ru5-250 and Ru5-450 samples. Figure 21 and Figure 22 concern the CO_2 capture step while Figure 23 and Figure 24 concern the methanation step.

Concerning first the capture stage three peaks are observed. A peak of gaseous CO_2 is apparent at around 2345 cm^{-1}, corresponding simply to the CO_2 injected to be captured. A second small peak corresponding to carbonyl species is observed at 1850 cm^{-1}. The carbonyl is formed at the Ru surface and corresponds to the dissociation of the CO_2 at this catalytic site. Finally, the last two peaks correspond to the bidentate carbonates. This corresponds to the CO_2 adsorbed on the basic sites. The first conclusion is that Ru plays a role in CO_2 capture via dissociation into adsorbed carbonyl species. Concerning the evolution over time, we can observe an increase of bidentate carbonates and carbonyl species. This corresponds to an increase in the quantity adsorbed over time. The notable difference between the two samples is a greater adsorption for Ru5-450.

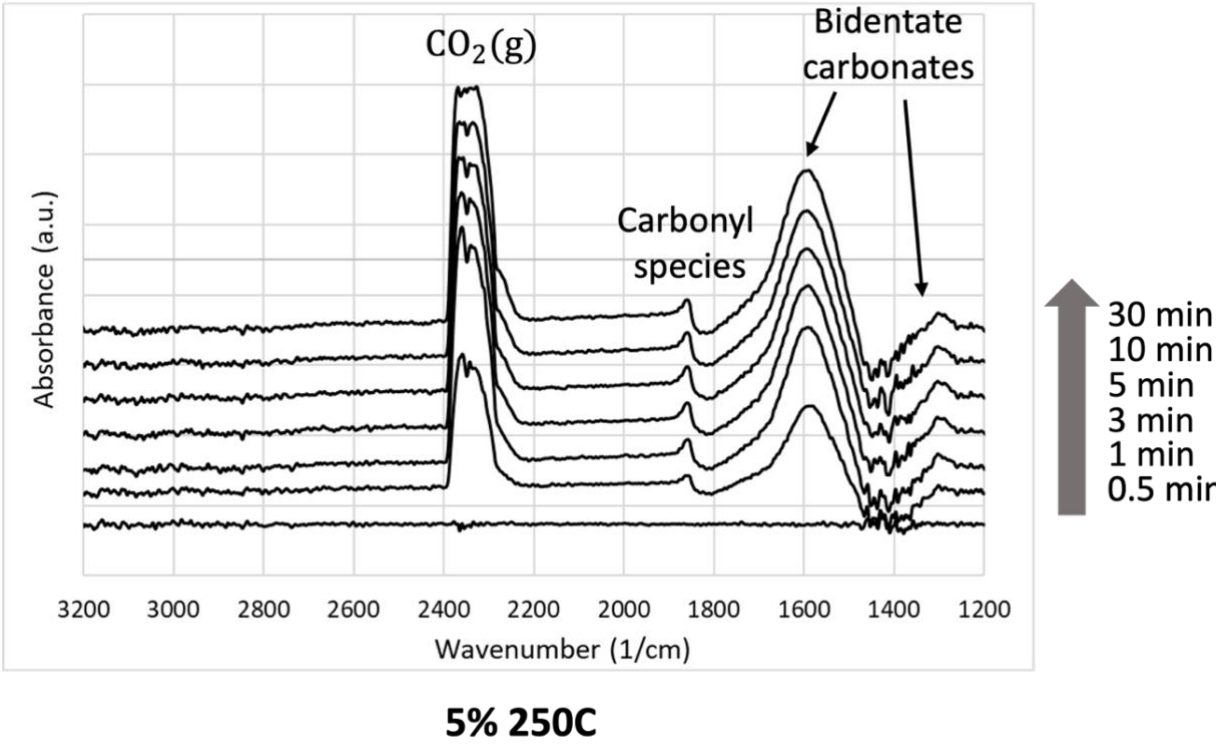

Figure 21 : In situ DRIFTS for Ru5-250 during capture step

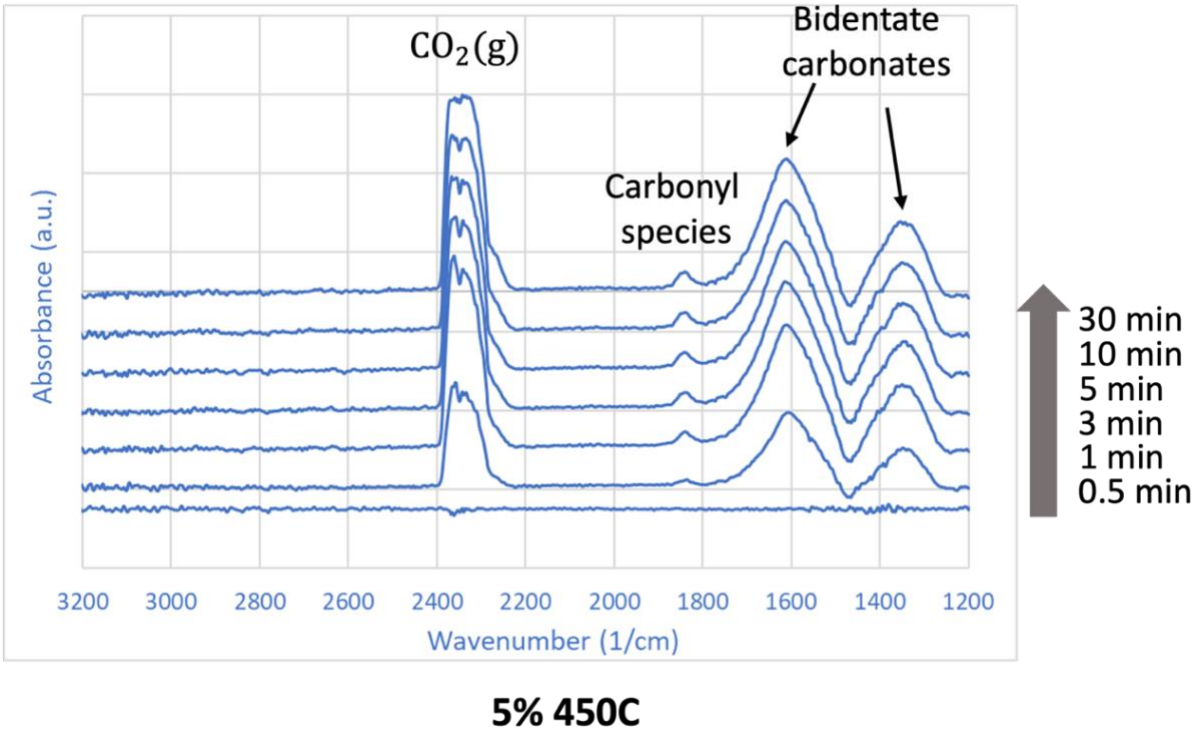

Figure 22 : In situ DRIFTS for Ru5-450 for capture step

During the methanation step the same peaks as previously mentioned are present with the addition of a peak corresponding to bicarbonates. The presence of gaseous CO_2 at this stage could be due to the presence of residues in the lines despite the flush stage or to CO_2 desorption from the DFM due to the exothermicity of the reaction. An unexpected negative carbonyl peak is observed for sample Ru5-250. By contrast, carbonyl peaks at 1960 and 1850 cm^{-1} are observable in the spectra of Ru5-450. These carbonyl species can be hydrogenated to CH_4. The presence of bicarbonate corresponds to a spillover of the CO_2 adsorbed on the basic sites to the Ru-support interface, at which they are further hydrogenated to methane with formate as intermediate species [31]. This spillover is promoted by the injection of hydrogen. In the course of time a decrease of the bidentate carbonates and an increase of the bicarbonates is observed. This is explained by the fact that bidentate carbonates formed on the basic sites are gradually desorbed in a first step with the help of the hydrogen injection to react at the catalytic site. As the reaction releases heat, it allows desorbing more of these bidentate carbonates. However, among this CO_2, a part is fixed on the support. This increase reflects the desorption process of CO_2. The absence of a peak corresponding to formate (intermediate formed by CO_2 hydrogenation) is due to its short lifetime as an intermediate. No peak is observed for methane, the product of the reaction, it is probably since it is produced in small quantities and therefore the peak is not visible. The two samples show similar profiles, but the reaction appears slower for the Ru5-250 sample.

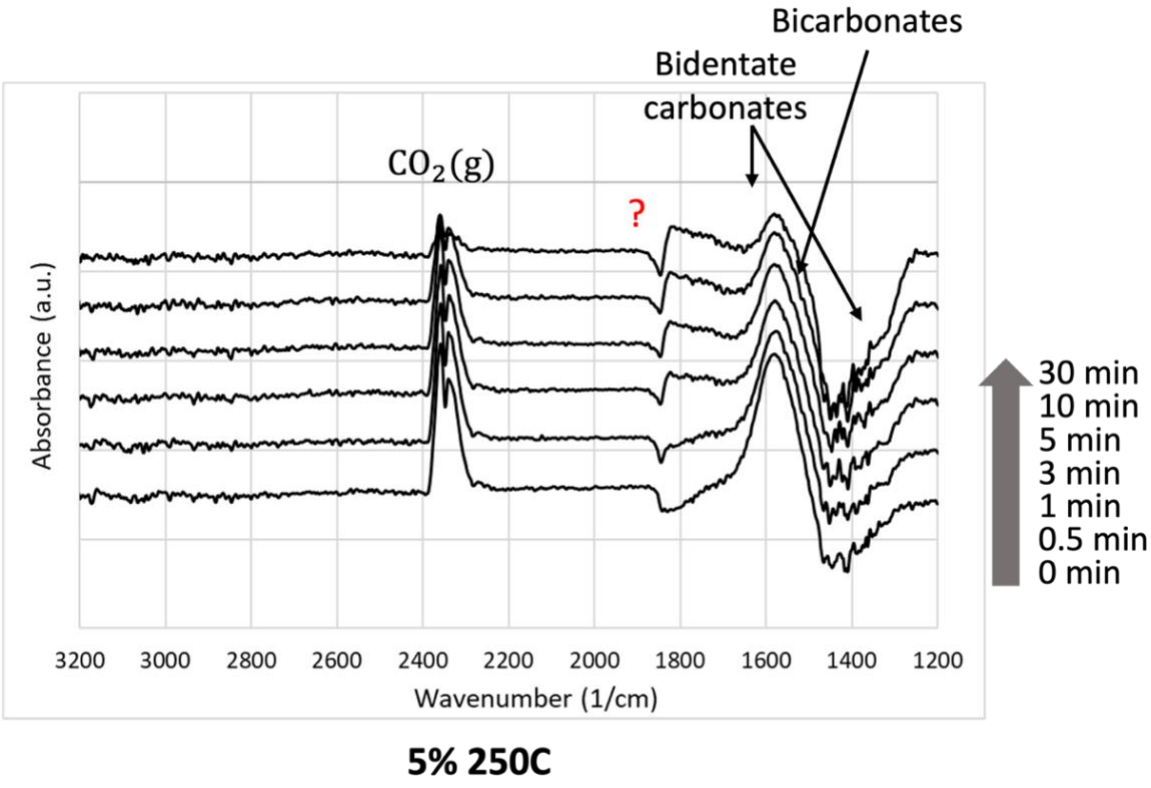

Figure 23 : In situ DRIFTS for Ru5-250 during methanation step

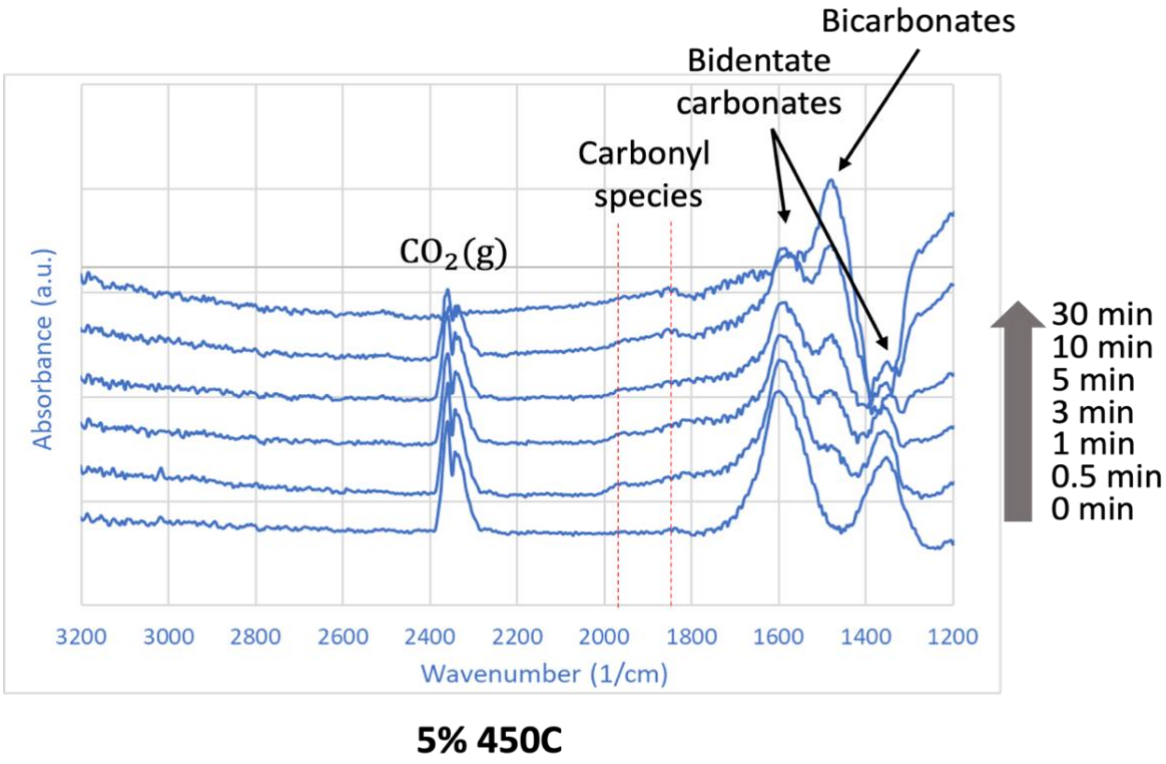

Figure 24 : In situ DRIFTS for Ru5-450 during methanation step

We can therefore conclude that the calcination temperature for Ru impregnation has no impact on the reaction pathway and does not notably change the interactions at the DFM surface.

Table 9 summarizes the different species identified, their structure and the wavelength(s) associated with their peak(s).

Table 9 : DRIFTS identified species and structures [31,42]

Species	**Bands (cm^{-1})**	**Structure**
Gaseous CO_2	2345	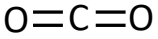
Carbonyl species	2000-1850	
Bidentate carbonates	1600 1370	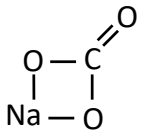
Bicarbonates	1650 1440	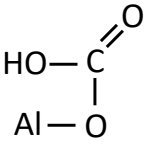

4.2 Optimizing DFM synthesis: Impact of ruthenium loading

4.2.1 N_2 physisorption

As expected from the results obtained in 4.1.1, no significant difference is observed in terms of textural properties depending on Ru loading. Indeed, similar physisorption isotherms are observed (Figure 25), as well as similar specific surface area and pore volume values (Table 10).

Note that this analysis was performed on 6% Na_2O–1,2,4,5% RuO_2/Al_2O_3 calcined at 350°C and not 450°C like the rest of this section. However, for this specific analysis it should not impact the results.

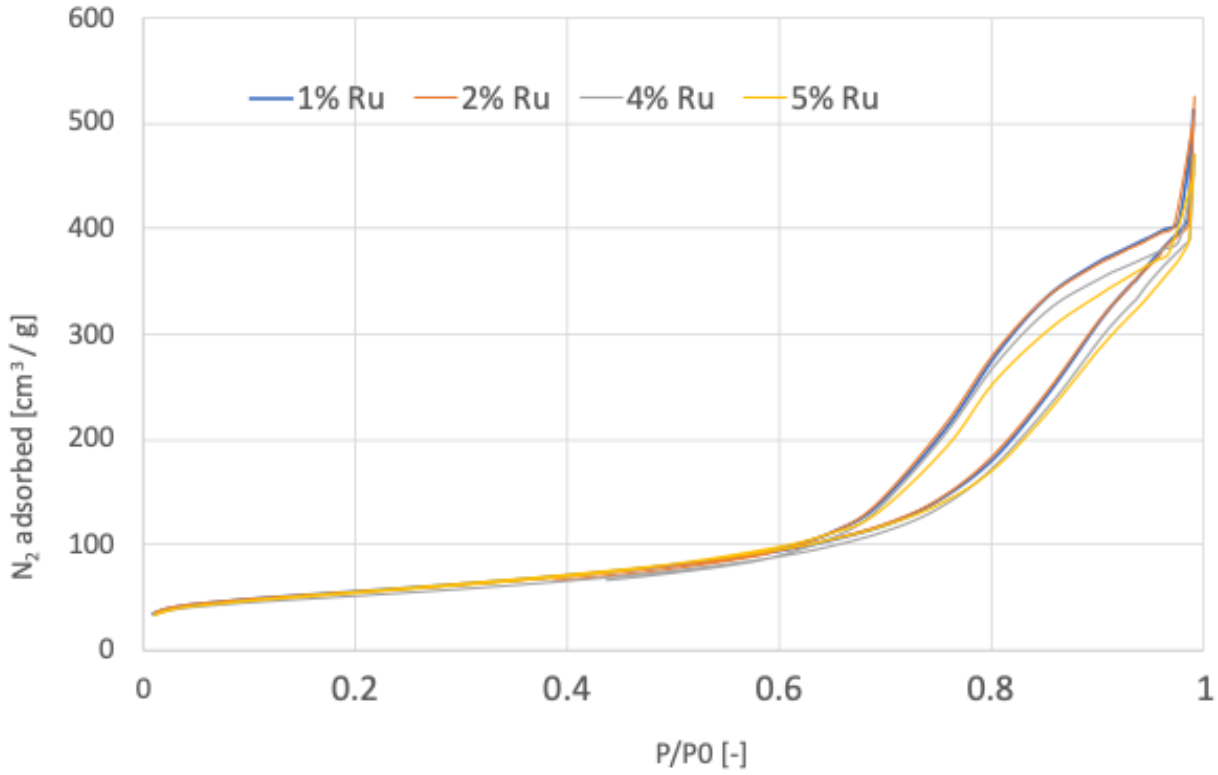

Figure 25 : N_2 physisorption isotherms for different Ru loadings

Table 10 : Textural properties for different Ru loadings

Ru loading (%)	1	2	4	5
BET surface area (m^2/g)	190	188	178	197
Pore volume (cm^3/g)	0.63	0.63	0.60	0.60

4.2.2 XRD

The diffractograms obtained by XRD for the different Ru loadings are shown in Figure 26 : XRD results for different Ru loadings. As before, RuO_2 (28°, 35° and 54°) and support (38°, 46° and 66°) peaks can be observed. For low loadings (1 and 2%), very small peaks are observed for RuO_2. This is due to the presence of too little RuO_2 to obtain strong peaks. For higher loadings (4 and 5%) sharper peaks are present.

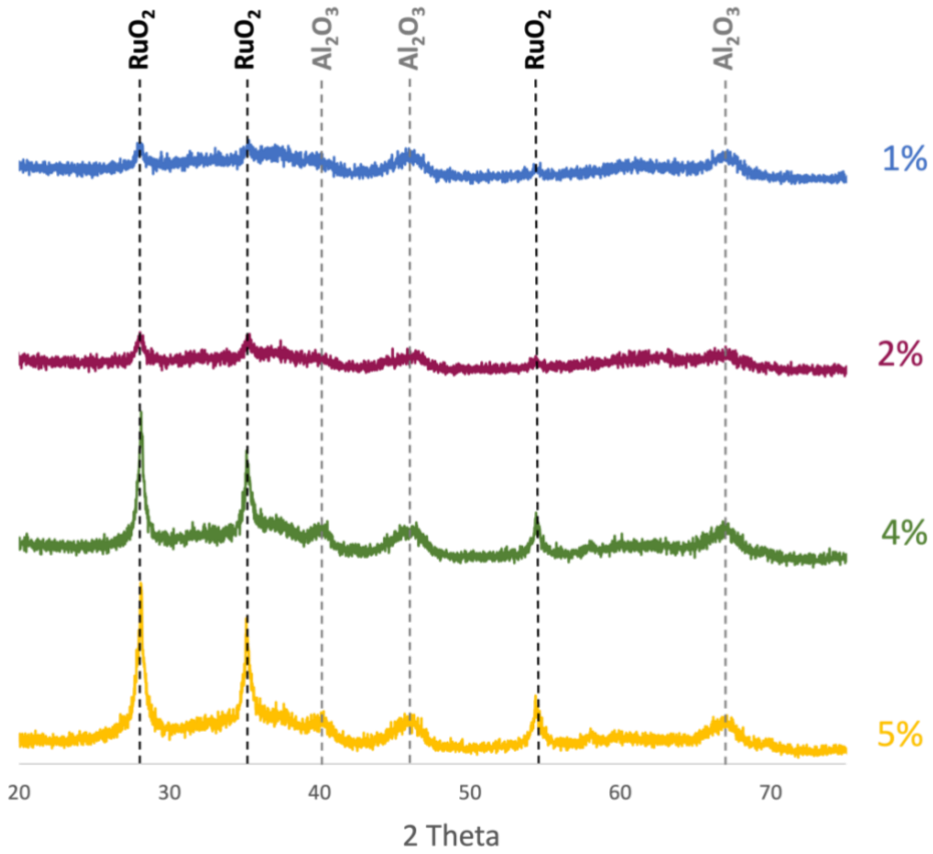

Figure 26 : XRD results for different Ru loadings

In terms of crystallite site size, 4% of Ru is larger than 5%. An average size of 252 Å is calculated for 4%, while a size of 197 Å is calculated for 5% (Table 11). Sizes have not been calculated for 1% and 2% due to the fading of peaks.

Table 11 : Size of crystallite sites for different Ru loadings

Ru loading (%)	**4**	**5**
(110)	229	177
(101)	186	218
(211)	340	195
Average size (Å)	**252**	**197**

Lastly, for spent catalysts (Figure 27), the metallic Ru peak (44°) is observed, as before, while the RuO_2 peak is more pronounced. Similar to the fresh samples, the Ru peaks are smaller for 1 and 2% than for 4 and 5%, once again reflecting the low number of catalytic sites at low loadings.

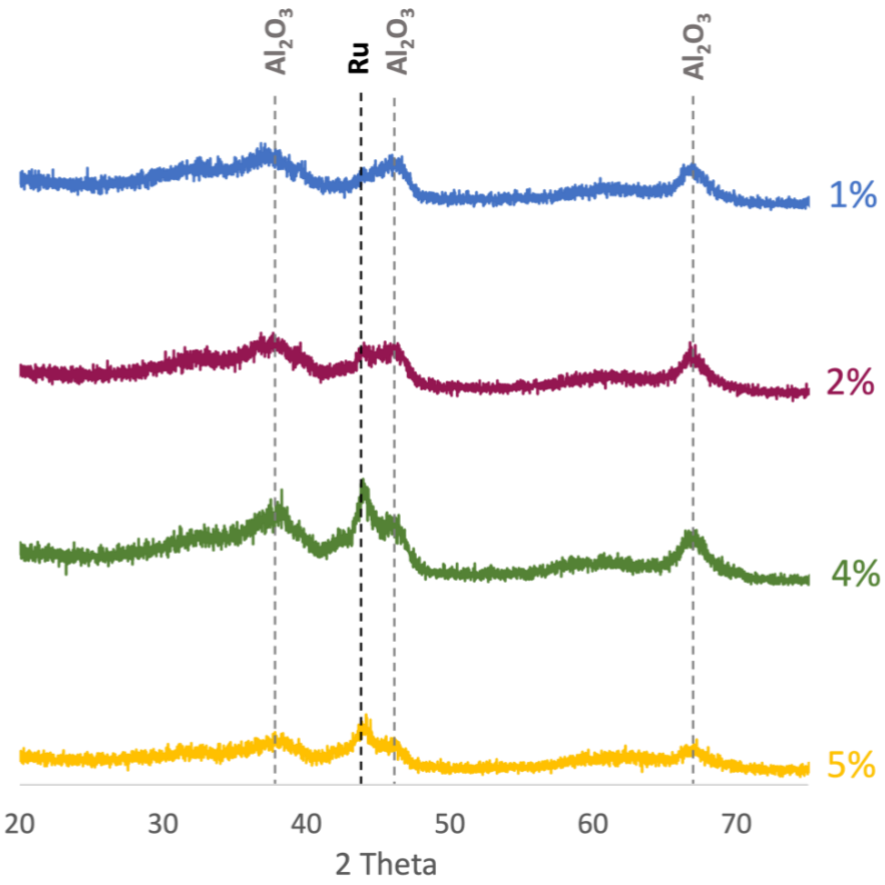

Figure 27 : XRD results for spent catalyst with different Ru loadings

4.2.3 CO_2 TPD

CO_2 TPD results for different Ru loadings (Figure 28) show the same two peaks as identified in 4.1.3. A similar profile is observed for the different samples. However, the 5% Ru sample shows a higher amount of CO_2 desorbed than the others for both the low-temperature and high-temperature peaks. This means that its low- and high-affinity adsorption sites adsorb more CO_2 than the other samples. The 4% Ru sample, on the other hand, shows a higher desorbed amount for the low-temperature peak. This indicates that its weakly interacting sites capture more CO_2. We therefore observe a tendency for samples containing more Ru to adsorb more CO_2. This indicates that CO_2 also adsorbs on Ru to a significant extent.

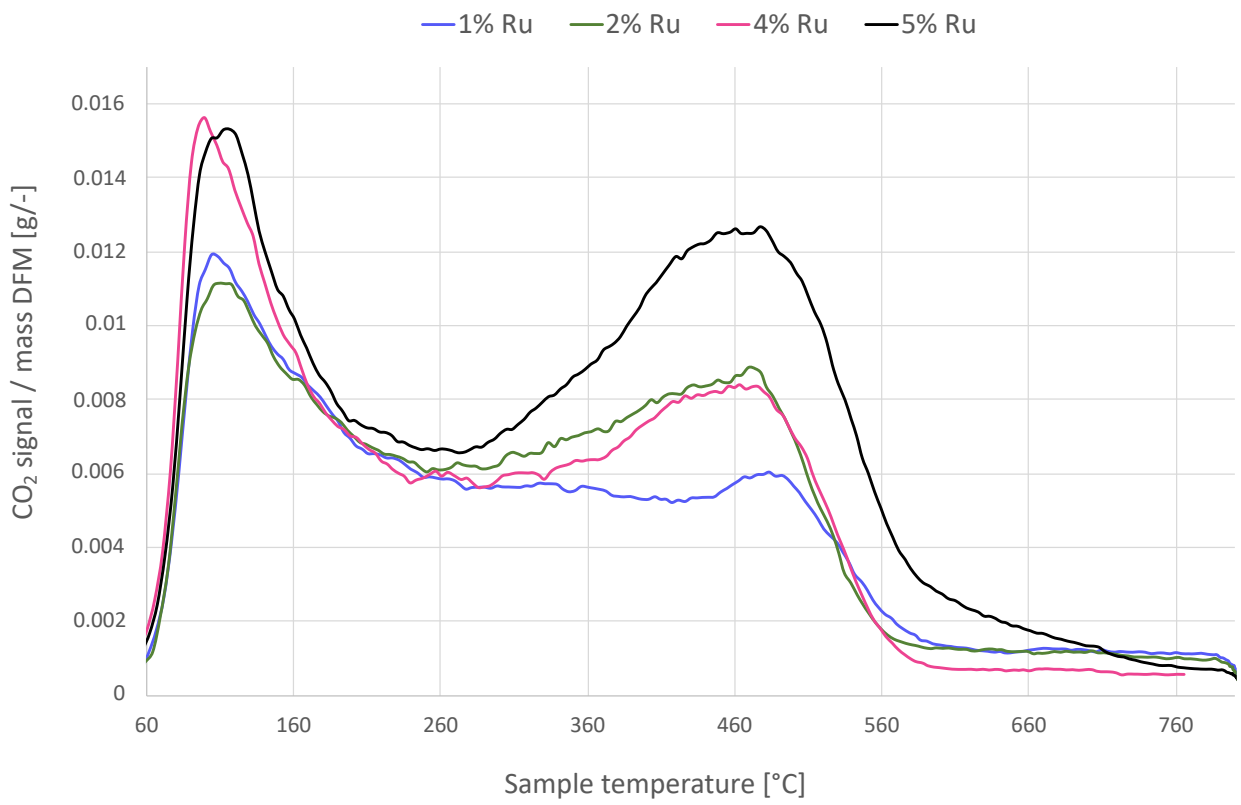

Figure 28 : CO_2 TPD for different Ru loadings

In order to confirm the role of Ru in CO_2 capture, CO_2 TPD results for a sample with Na and Ru were compared with a sample with only Na and a sample with only Ru (Figure 29). Comparing the sample with basic sites only with the sample with catalytic sites only, the adsorption on the sample with Na is much higher. However, both desorption peaks are still observed, as previously observed in the other samples for the sample with Ru only. If we compare the sample with Ru and Na with the one with Na only, we see that the peak at higher temperature is greater for the sample containing also Ru. We can therefore conclude that the addition of Ru increases the number of CO_2 capture sites from medium to strong interaction. This is of interest for the methanation reaction, given that these are the same sites that are solicited.

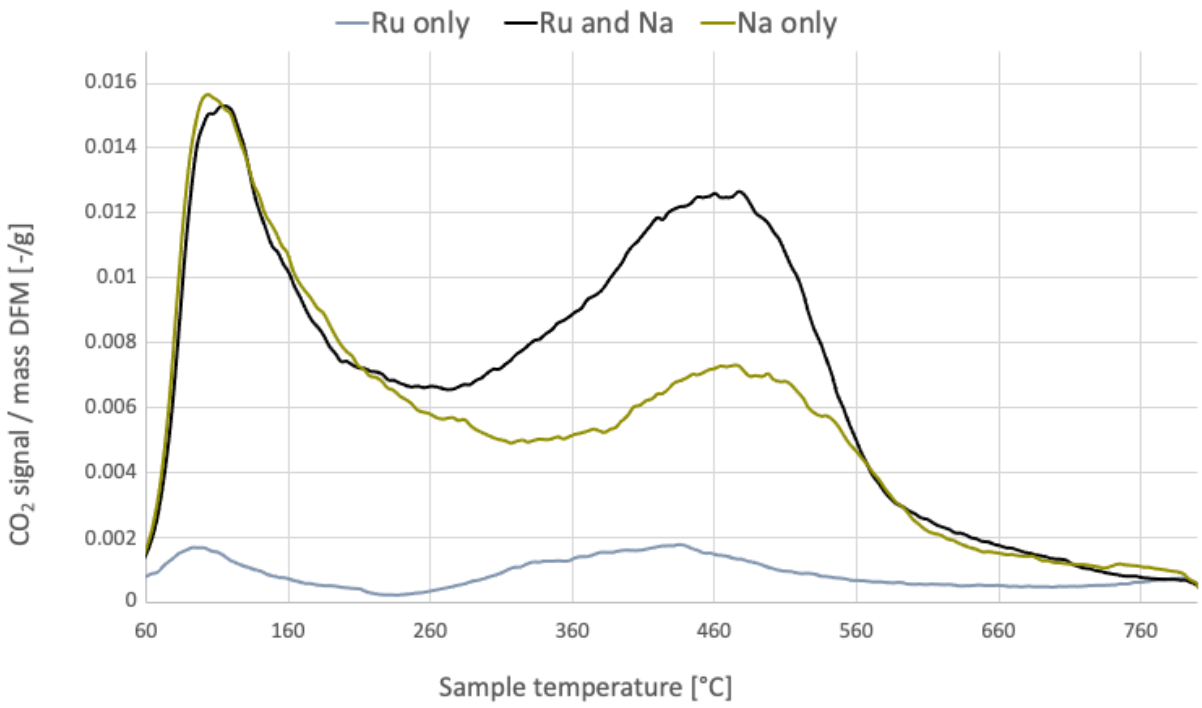

Figure 29 : CO_2 TPD for different types of sites

4.2.4 Catalytic testing

The results of the catalytic tests for the different Ru loadings are shown in Table 1. As the results for the 2% Ru sample are not consistent between the three cycles, they will not be discussed here and are presented for informational purposes only. This sample has a high conversion rate but captures very variable amounts of CO_2 depending on the cycle (0.05 moles/kg DFM for cycle 1, 0.10 moles/kg DFM for cycle 2 and 0.17 moles/kg DFM for cycle 3). This suggests that the problem may relate to the experimental conditions during catalytic testing. For the other DFMs, there is a clear trend towards better performance at loadings of 4-5% Ru compared with 1% Ru. In fact, the amount of CO_2 captured and the amount of methane produced are greater for the 4% and 5% Ru samples. Regarding conversion rates, this trend is reversed. However, calculating the amount of methane produced is more reliable than calculating the amount of CO_2 captured. The calculation of the amount of methane produced is straightforward (directly calculated from the area obtained from the MS), but the calculation of the amount of CO_2 captured is not (see 3.2.3 Catalytic testing). We therefore prefer to focus on the amount of methane produced per unit mass of DFM to determine which DFM is the most efficient, rather than the conversion rate.

Table 12 : Catalytic testing results for different Ru loadings

Catalyst	**CO_2 captured (moles/kg DFM)**	**Methane produced (moles/kg DFM)**	**Conversion (%)**
Ru1-450	0.10	0.08	80
Ru2-450	0.14	0.13	95
Ru4-450	0.18	0.13	75
Ru5-450	0.21	0.13	62

As before, methane production profiles as a function of time can be studied to highlight any differences in the speed of methane production for DFMs producing similar quantities. These profiles represent the helium-normalized methane signal for which the baseline has been adjusted, over a period of 1000 seconds and are presented in figure 1. We can observe a much smaller peak for the DFM with 1% Ru than for the other samples. This is to be expected, given that this sample produces less methane. For the samples with 4 and 5% Ru producing similar quantities of methane, the production profiles are similar. This means that there is no difference in efficiency, either in terms of quantity or speed, between these two samples.

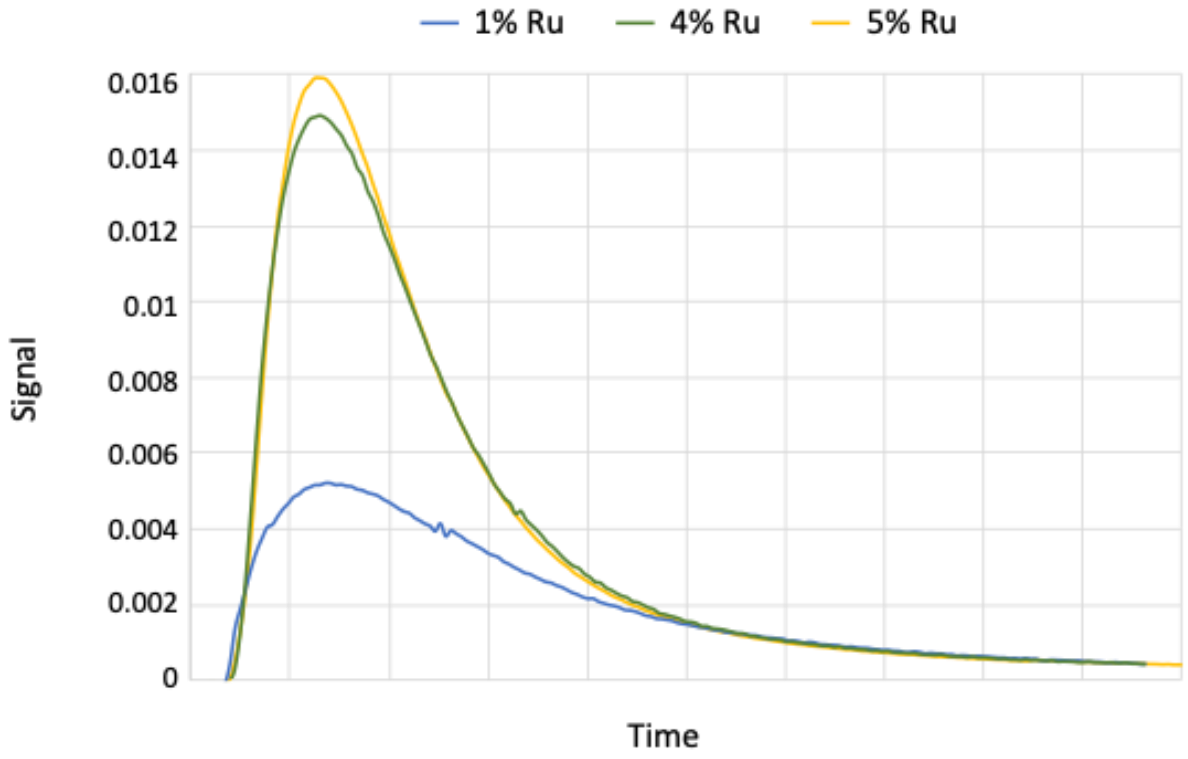

Figure 30 : CH_4 production profile for different Ru loadings

4.2.5 DRIFTS

The profiles obtained by DRIFTS over time are shown in Figure 31 and Figure 32 for the capture step for samples Ru2-450 and Ru5-450 respectively, and in Figure 33 and Figure 34 for the methanation step for the same samples.

For the CO_2 capture step, the same species are observed as before: gaseous CO_2, carbonyl species corresponding to CO_2 dissociated on Ru sites, and bidentate carbonates corresponding to CO_2 adsorption on basic sites. Both samples show an increase in carbonyl and bidentate carbonate species over time. This corresponds to an increase in the amount of CO_2 adsorbed by DFM over time. The amount of bidentate carbonate is similar for both samples. This can be explained by the fact that these species correspond to adsorption on basic sites, and the percentage of basic sites is 6% for both samples. However, the amount of carbonyl is greater in the sample with 5% Ru. This is to be expected, given that this species corresponds to CO_2 dissociation on Ru sites, and thus more Ru means more carbonyl formation on these sites.

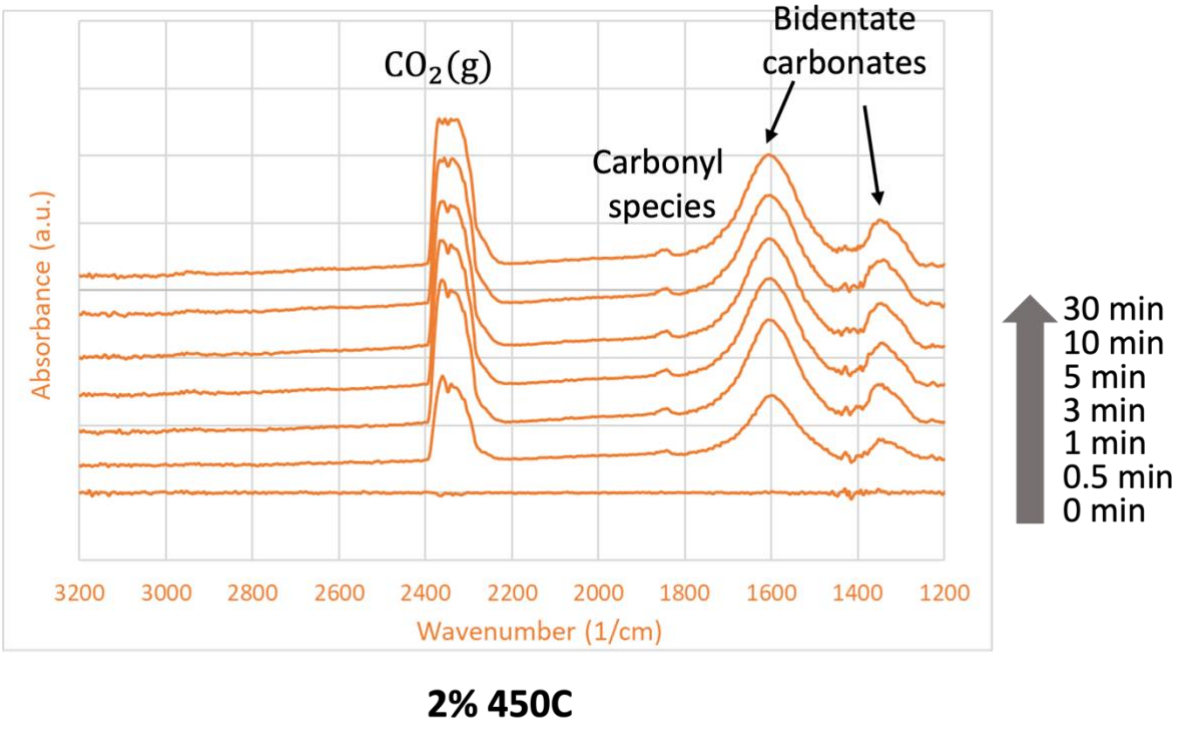

Figure 31 : In situ DRIFTS for Ru2-450 during capture step

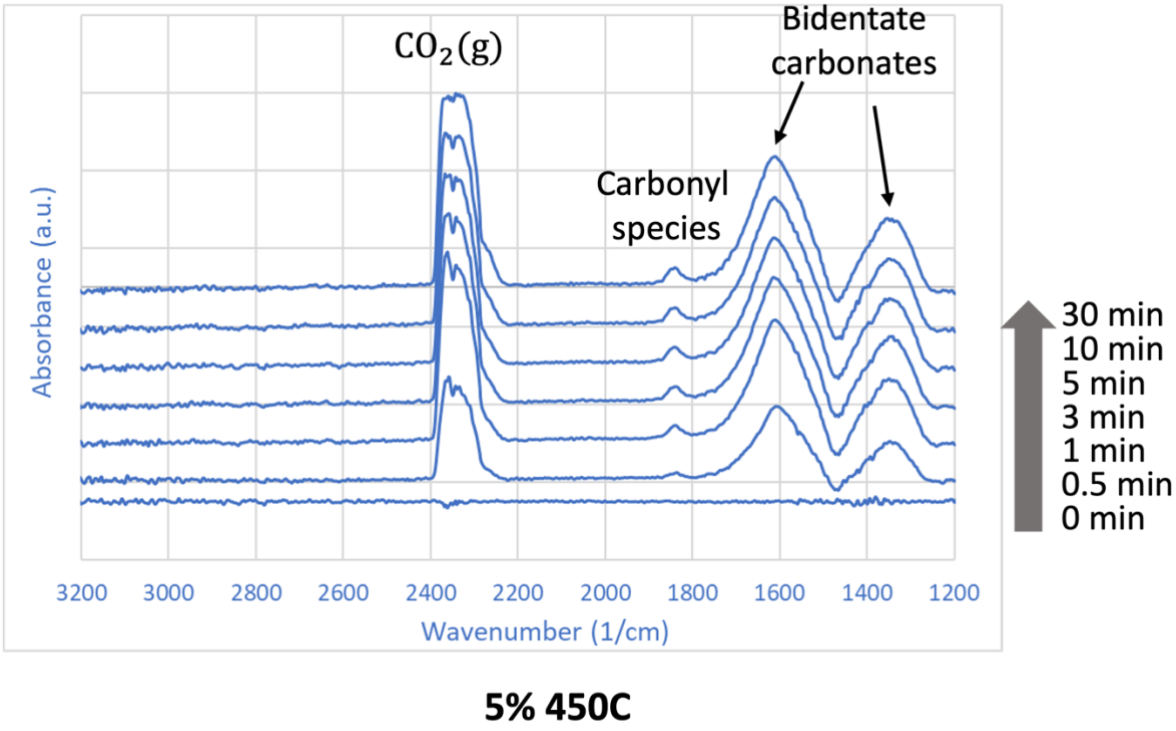

Figure 32 : In situ DRIFTS for Ru5-450 during capture step

The methanation step involves the same species as before, plus a peak corresponding to bicarbonates. The presence of gaseous CO_2 at this stage of the reaction is explained by its presence in the pipes despite the flush stage or the presence of hotspots allowing CO_2 desorption from the DFM. Bicarbonates correspond to the adsorption of CO_2 on the Ru-support interface. This is due to the spill-over of CO_2 from the basic sites as a result of both the injection of hydrogen and the release of heat by the methanation reaction. Over time, a decrease in bidentate carbonates and an increase in bicarbonates is observed, corresponding to the spillover phenomenon explained above, which becomes stronger as the reaction progresses. More bicarbonates are formed on the sample with 5% Ru than on the one with 2% Ru. Likewise, as in the previous step, more carbonyls are observed in the sample with 5% Ru than in that with 2% Ru, as carbonyls are formed on Ru. The reaction is also slower for the 2% Ru sample. This is due to the fact that the Ru sites are both CO_2 dissociation sites and hydrogen dissociation sites. When there is less Ru, there is less dissociated CO_2 available for reaction, but more importantly, there is less dissociated hydrogen available for reaction. This leads to slower progress in the methanation reaction.

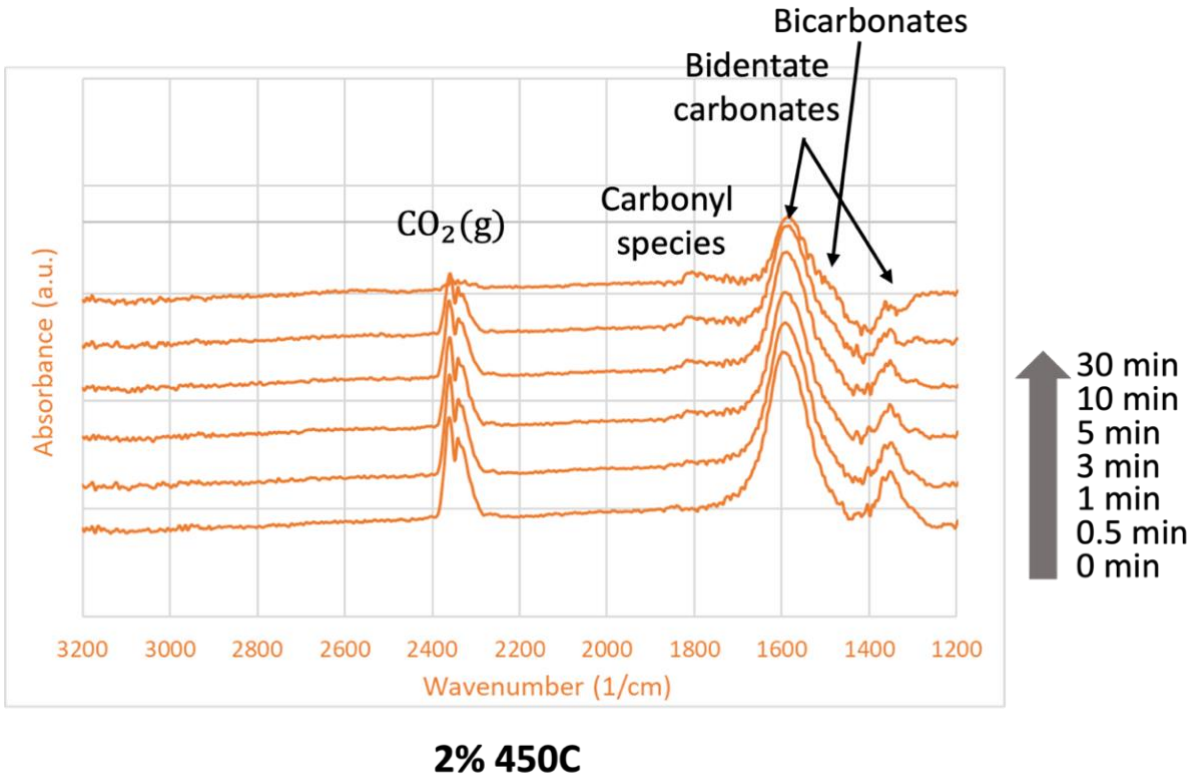

Figure 33 : DRIFTS for Ru2-450 during methanation step

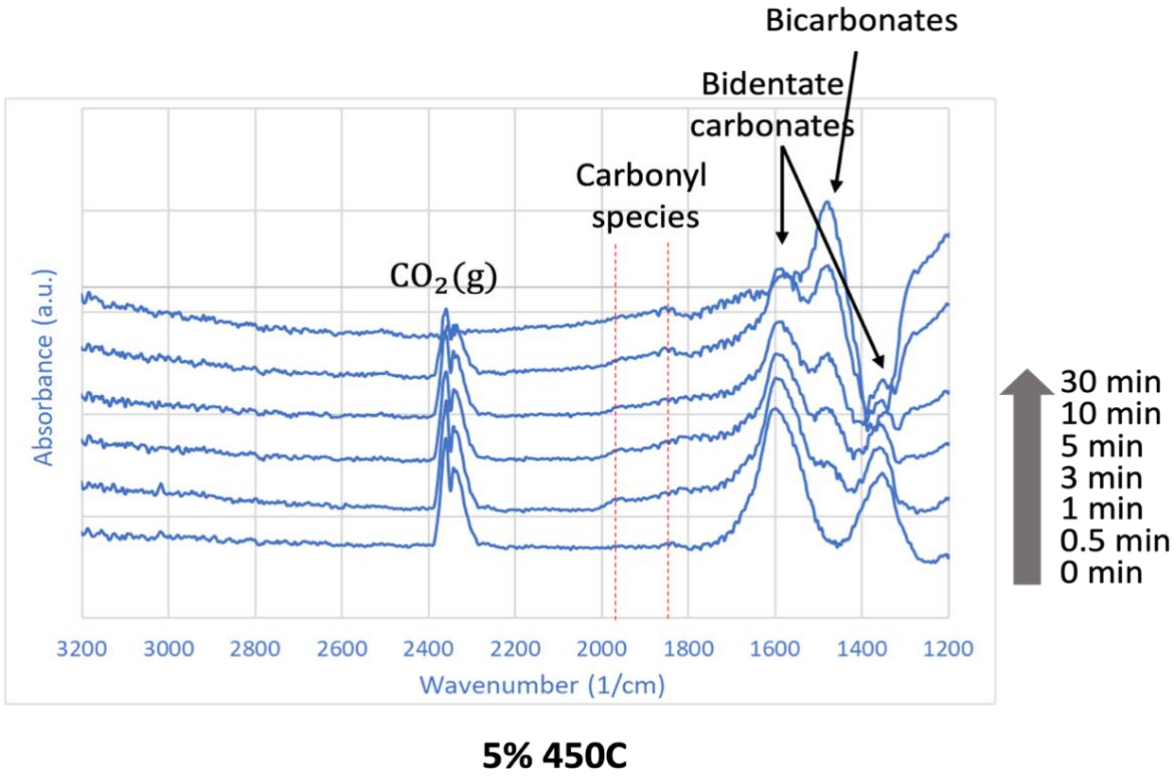

Figure 34 : DRIFTS for Ru5-450 during methanation step

In summary, this analysis shows that the presence of more Ru sites in the DFM leads to greater adsorption of CO_2, but also to more hydrogen dissociation, resulting in a faster methanation reaction.

Details of the structures and bands of the various species identified are given in Table 9.

5 Discussion

This section presents a discussion of the results obtained, as well as a link between the different analysis methods and their results.

5.1 Impact of calcination temperature for second impregnation

5.1.1 XRD – catalytic testing results

The XRD analysis highlighted two elements. Firstly, the presence of $NaNO_3$ resulting from a side reaction for samples calcined at 200 and 250°C was observed. Secondly, by calculating the size of the crystallite sites, it was observed that Ru5-200 had smaller crystallite sites and that calcination temperature above that resulted in bigger crystallite sites.

The presence of $NaNO_3$ on DFMs calcined at low temperatures raises the question of its interference with basic capture sites. However, the results of the catalytic tests show that no marked difference in terms of CO_2 capture is observed between samples containing $NaNO_3$ (Ru5-200 and Ru5-250) and samples in which it is not present (Ru5-350 and Ru5-450). Moreover, the CO_2 TPD shows no difference between these samples in terms of CO_2 capture capacity. It can therefore be concluded that the presence of this species does not influence the efficiency of the DFMs.

Calculation of the crystallites site size using the Scherrer equation showed that the Ru5-250, Ru5-350 and Ru5-450 samples had larger Ru crystallite sites than the Ru5-200 samples. However, the results of the catalytic testing showed no marked difference between these two groups of samples. It can therefore be concluded that the difference in average size observed does not induce any difference in terms of DFM efficiency and thus that the differences in term of particle sizes resulting from higher calcination temperatures does not impact catalyst performance in the range of temperatures tested.

5.1.2 CO_2 TPD – catalytic testing results

CO_2 TPD shows slightly higher capture for Ru5-350 and slightly lower capture for Ru5-200 in the area of interest for the reaction (medium to strong basic sites), compared with the other samples. The catalytic testing shows a slightly lower capture for Ru5-250 compared with the other samples, which show similar capture rates. It can therefore be concluded that these differences in CO_2 capture capacity are minor, and that the calcination temperature for the second impregnation has no impact on the DFMs CO_2 capture capacity.

5.1.3 DRIFTS – catalytic testing results

DRIFTS analysis shows that the different samples have a similar capture and reaction pathway. This matches the results of the catalytic test, which showed no marked differences between samples. DRIFTS results suggest a slower reaction for Ru5-250 compared with Ru5-450. This corresponds to the results obtained for these samples in the catalytic test. In fact, Ru5-450 captures more CO_2 and produces more methane in the catalytic testing than Ru5-250.

5.1.4 Ru volatilization at high temperature

Proaño et al. [31] suggested that calcination temperatures in excess of 250°C should be avoided for Ru impregnation, as this would cause RuO_2 volatilization. Indeed, at high temperatures, RuO_2 lead to the formation of toxic volatile species (RuO_4 and/or RuO_3)[43]. However, the results of the XRD and catalytic tests in particular suggest that in the temperature range used (200°C to 450°C) RuO_2 volatilization is not a problem. Indeed, the diffractogram confirms the presence of RuO_2 in all samples, with no obvious differences. The catalytic testing even shows slightly better results at higher temperatures (350°C and 450°C), and if less Ru were present in these samples, less methane would be produced compared to the samples calcined at lower temperature. However, to confirm that there is no volatilization of RuO_2, ICP (Inductively Coupled Plasma) spectroscopy should be carried out to define the composition of the different DFMs more precisely [44].

5.1.5 Optimal second impregnation calcination temperature

As demonstrated by the various analyses, the calcination temperatures tested had no major impact on DFMs efficacy and characteristics. For the remainder of the work, it was decided to work with a DFM calcined at 450°C, as this sample produced slightly more methane than the other samples and contained no $NaNO_3$. However, the presence of $NaNO_3$ was also shown to have no major impact. In the context of an industrial application of this technology, however, it would be more interesting to use a lower temperature, given that no major differences were observed, and in order to reduce energy consumption.

5.2 Impact of ruthenium loading

5.2.1 XRD – catalytic testing results

XRD reveals a size difference between the Ru4-450 and Ru5-450 crystal sites. Ru4-450 has an average crystalline site size of 252 Å, whereas Ru5-450 has an average size of 197 Å. The catalytic tests for these two samples show similar results in terms of CO_2 capture and methane production, suggesting that the average size of the crystalline sites has no impact on DFM efficiency. To be sure, methane production profiles of the catalytic tests can be compared. These profiles are similar for both samples, confirming similar efficiencies.

5.2.2 Role of Ruthenium in CO_2 capture

As observed via the catalytic tests, samples with more Ru (Ru4-450 and Ru5-450) give better results in terms of methane production than samples with less Ru (Ru1-450 and Ru2-450). This result is expected given that Ru is the catalytic site for the methanation reaction, allowing hydrogen to dissociate and react with the dissociated CO_2. More Ru speeds up the reaction and maximizes the amount of CO_2 converted into methane. However, we also observe that samples with more Ru show better results in terms of CO_2 capture (via CO_2 TPD and catalytic test), which also plays a role in the fact that they produce more methane. The role played by ruthenium in CO_2 capture was first highlighted by comparing CO_2 TPD results for DFM and samples with only basic site and only catalytic site. This showed that the addition of ruthenium increases the adsorption capacity of CO_2 on sites that are solicited during the reaction. DRIFTS were then used to gain a better understanding of the mechanism. DRIFTS showed that during the capture step, CO_2 dissociated directly on the ruthenium in carbonyl form, thus increasing the amount of adsorbed CO_2. Additionally, more ruthenium sites may facilitate a spillover of bidentate carbonates into the Ru-support interface, at which methanation takes place via sequential hydrogenation with formate as intermediate species.

5.2.3 Optimal ruthenium loading

Among the different percentages tested, we can observe that higher loadings (Ru4-450 and Ru5-450) give better results than lower loadings. However, this doesn't mean that even higher loadings would give even better results. Indeed, beyond a certain loading for a constant percentage of basic sites, all the CO_2 will already be transformed, so further increasing Ru loading would no longer increase performance. It would also be interesting in this case to carry out ICP spectroscopy to define the actual Ru loading more precisely, given that we're working at very low loading.

6 Conclusion

This work focuses on the use and optimization of DFMs for the capture of CO_2 and its conversion into methane to address current climate issues. The DFMs used for this purpose have Na_2O as basic sites and Ru nanoparticles as catalytic sites, both supported on gamma alumina. They are synthesized by two successive wet impregnations. In this work, two aspects of DFM synthesis were studied in order to optimize the material.

First, different calcination temperatures for Ru impregnation were tested in order to understand how it impact Ru particle size and its effect on catalytic performances. Four temperatures were tested, ranging from 200 to 450°C. XRD analysis pointed out that Ru5-200 resulted in smaller particle size than temperatures above that. Catalytic testing showed no markable difference between the methane production and CO_2 capture of the samples. It can therefore be concluded that calcination temperature has no impact on DFM capabilities in the range tested. XRD revealed the presence of $NaNO_3$, a by-product, in DFMs calcined at 200 and 250°C, but CO_2 TPD and catalytic testing did not point to any marked influence of this species on DFM performance. Finally, it was demonstrated that temperatures up to 450°C do not cause RuO_2 volatilization.

Next, the effect of varying ruthenium loading was studied. To this end, DFMs with 1, 2, 4 and 5% ruthenium loading were studied. Catalytic tests have shown that samples with 1 and 2% loading are significantly less efficient than those with 4 and 5%. This is primarily due to the fact that ruthenium is the reaction site, so having more ruthenium enables more CO_2 to be converted. But also because ruthenium is involved in CO_2 adsorption during the capture stage. Indeed, CO_2 TPD and DRIFTS have highlighted the ability of CO_2 to dissociate on ruthenium. Having more ruthenium means capturing more CO_2, and therefore naturally producing more methane.

7 Bibliography

1. IPPC. *Synthesis report of the IPPC sixth assessment report*. https://report.ipcc.ch/ar6syr/pdf/IPCC_AR6_SYR_LongerReport.pdf.
2. Copernicus. *Climate indicators - temperature*. https://climate.copernicus.eu/climate-indicators/temperature (2023).
3. GIEC. *Réchauffement planétaire de 1,5°C*. (2019).
4. Qu'est-ce que la neutralité carbone et comment l'atteindre d'ici 2050 ? *Parlement Européen* https://www.europarl.europa.eu/news/fr/headlines/society/20190926STO62270/qu-est-ce-que-la-neutralite-carbone-et-comment-l-atteindre-d-ici-2050 (2019).
5. How carbon-intensive industries can scale up CO2 recycling | Research and Innovation. https://ec.europa.eu/research-and-innovation/en/horizon-magazine/how-carbon-intensive-industries-can-scale-co2-recycling.
6. Lv, Z. *et al.* Integrated CO2 capture and In-Situ methanation by efficient dual functional Li4SiO4@Ni/CeO2. *Sep. Purif. Technol.* **309**, 123044 (2023).
7. Paulina Melo Bravo & Damien Debecker. Combining CO2 capture and catalytic conversion to methane. Waste Dispos. Sustain. Energy,1, 53-65 (2019).
6. REN21, *Renewables Global Futures Report: Great debates towards 100% renewable energy* (2017)
9. Liu, J. *et al.* Life cycle cost modelling and economic analysis of wind power: A state of art review. *Energy Convers. Manag.* **277**, 116628 (2023).
10. Ali, N. *et al.* Thermochemical and electrochemical aspects of carbon dioxide methanation: A sustainable approach to generate fuel via waste to energy theme. *Sci. Total Environ.* **712**, 136482 (2020).
11. Parsons, A. Europe must diversify its renewable energy supply to avoid future shocks. *Ocean Energy Europe* https://www.oceanenergy-europe.eu/res-diversity/ (2021).
12. Sun, J., Zhao, M., Huang, L., Zhang, T. & Wang, Q. Recent progress on direct air capture of carbon dioxide. *Curr. Opin. Green Sustain. Chem.* **40**, 100752 (2023).
13. Cuéllar-Franca, R. M. & Azapagic, A. Carbon capture, storage and utilisation technologies: A critical analysis and comparison of their life cycle environmental impacts. *J. CO2 Util.* **9**, 82–102 (2015).
14. Han, Y. & Ho, W. S. W. Polymeric membranes for CO2 separation and capture. *J. Membr. Sci.* **628**, 119244 (2021).
15. Bi, Y. & Ju, Y. Design and analysis of CO2 cryogenic separation process for the new LNG purification cold box. *Int. J. Refrig.* **130**, 67–75 (2021).
16. Liu, Y. *et al.* Ionic liquids/deep eutectic solvents for CO2 capture: Reviewing and evaluating. *Green Energy Environ.* **6**, 314–328 (2021).
17. Song, Y. *et al.* Geomechanical challenges during geological CO2 storage: A review. *Chem. Eng. J.* **456**, 140968 (2023).

18. Thomas Len & Rafael Luque. Addressing the CO2 challenge through thermocatalytic hydrogenation to carbon monoxide, methanol and methane. Green Chem., 25, 490-521 (2023).
19. Hasan, M. M. F. *et al.* Can CO2 and Renewable Carbon Be Primary Resources for Sustainable Fuels and Chemicals? *ACS Sustain. Chem. Eng.* **9**, 12427–12430 (2021).
20. Chatzilias, C., Martino, E., Katsaounis, A. & Vayenas, C. G. Electrochemical promotion of CO2 hydrogenation in a monolithic electrochemically promoted reactor (MEPR). *Appl. Catal. B Environ.* **284**, 119695 (2021).
21. Cabrero-Antonino, M. *et al.* Solar-driven gas phase photocatalytic CO2 methanation by multimetallic UiO-66 solids decorated with RuOx nanoparticles. *Chem. Eng. J.* **468**, 143553 (2023).
22. Jiang, H., Hao, W., Li, Y. & Zhou, H. Biological methanation of H2 and CO2 in a continuous stirred tank reactor. *J. Clean. Prod.* **370**, 133518 (2022).
23. Fan, W. K. & Tahir, M. Recent trends in developments of active metals and heterogenous materials for catalytic CO2 hydrogenation to renewable methane: A review. *J. Environ. Chem. Eng.* **9**, 105460 (2021).
24. Loccufier, E. *et al.* CO2 methanation with Ru@MIL-101 nanoparticles fixated on silica nanofibrous veils as stand-alone structured catalytic carrier. *Appl. Catal. B Environ.* **320**, 121972 (2023).
25. Kim, A. *et al.* CO2 methanation on Ru/TiO2 catalysts: On the effect of mixing anatase and rutile TiO2 supports. *Appl. Catal. B Environ.* **220**, 615–625 (2018).
26. Mesoporous TiO2 Support Materials for Ru-Based CO2 Methanation Catalysts | ACS Applied Nano Materials. https://pubs.acs.org/doi/abs/10.1021/acsanm.9b00518.
27. Faria, A. C. *et al.* Cyclic operation of CO2 capture and conversion into methane on Ni-hydrotalcite based dual function materials (DFMs). *J. CO2 Util.* **72**, 102476 (2023).
28. Porta, A., Matarrese, R., Visconti, C. G., Castoldi, L. & Lietti, L. Storage Material Effects on the Performance of Ru-Based CO2 Capture and Methanation Dual Functioning Materials. *Ind. Eng. Chem. Res.* **60**, 6706–6718 (2021).
29. Zhang, L., Li, L., Zhang, Y., Zhao, Y. & Li, J. Nickel catalysts supported on MgO with different specific surface area for carbon dioxide reforming of methane. *J. Energy Chem.* **23**, 66–72 (2014).
30. Zheng, Q., Farrauto, R. & Chau Nguyen, A. Adsorption and Methanation of Flue Gas CO $_2$ with Dual Functional Catalytic Materials: A Parametric Study. *Ind. Eng. Chem. Res.* **55**, 6768–6776 (2016).
31. Proaño, L. *et al.* In-situ DRIFTS study of two-step CO2 capture and catalytic methanation over Ru,"Na2O"/Al2O3 Dual Functional Material. *Appl. Surf. Sci.* **479**, 25–30 (2019).
32. Aramouni, N. A. K., Zeaiter, J., Kwapinski, W., Leahy, J. J. & Ahmad, M. N. Trimetallic Ni-Co-Ru catalyst for the dry reforming of methane: Effect of the Ni/Co ratio and the calcination temperature. *Fuel* **300**, 120950 (2021).

33. Li, T., Wang, S., Gao, D. & Wang, S. Effect of support calcination temperature on the catalytic properties of Ru/Ce0.8Zr0.2O2 for methanation of carbon dioxide. *J. Fuel Chem. Technol.* **42**, 1440–1446 (2014).
34. Malins, K. & Malina, I. The effects of supported Pd, Pt, Re, Rh, Ru, Ir, Au, and Ni catalysts on renewable hydrocarbon production from alternative feedstock. *Biomass Bioenergy* **171**, 106732 (2023).
35. Jeong-Potter, C., Zangiabadi, A. & Farrauto, R. Extended aging of Ru-Ni, Na2O/Al2O3 dual function materials (DFM) for combined capture and subsequent catalytic methanation of CO2 from power plant flue gas. *Fuel* **328**, 125283 (2022).
36. Dabbagh, H. A., Yalfani, M. & Davis, B. H. An XRD and Fourier-transformed infrared spectroscopy investigation of single and mixed γ-alumina and thorium oxide. *J. Mol. Catal. Chem.* **238**, 72–77 (2005).
37. Prasanna, U. *et al.* Electrical, transport, and optical properties of a novel PVB-NaNO3 complexed solid polymer electrolyte thin-films for solid-state battery. *Mater. Today Proc.* (2023) doi:10.1016/j.matpr.2023.04.187.
38. Hoshino, Y., Utsunomiya, T. & Abe, O. The Thermal Decomposition of Sodium Nitrate and the Effects of Several Oxides on the Decomposition. *Bull. Chem. Soc. Jpn.* **54**, 1385–1391 (1981).
39. Nguyen-Quang, M. *et al.* Unveiling the potential of surfactant Pluronic-P123 application during the synthesis of Ni-hydrotalcite-derived catalysts for low-temperature CO2 methanation: A novel approach. *Appl. Mater. Today* **32**, 101805 (2023).
40. Jia, X., Zhang, X., Rui, N., Hu, X. & Liu, C. Structural effect of Ni/ZrO2 catalyst on CO2 methanation with enhanced activity. *Appl. Catal. B Environ.* **244**, 159–169 (2019).
41. Hongmanorom, P., Ashok, J., Chirawatkul, P. & Kawi, S. Interfacial synergistic catalysis over Ni nanoparticles encapsulated in mesoporous ceria for CO2 methanation. *Appl. Catal. B Environ.* **297**, 120454 (2021).
42. Di Cosimo, J. I., Díez, V. K., Xu, M., Iglesia, E. & Apesteguía, C. R. Structure and Surface and Catalytic Properties of Mg-Al Basic Oxides. *J. Catal.* **178**, 499–510 (1998).
43. Samed, A. J., Yamamoto, Y., Hidaka, M., Hinokuma, S. & Machida, M. An attempt to stabilize supported Ru catalysts against oxidative volatilization. *Catal. Commun.* **91**, 6–9 (2017).
44. ICP-MS as a Technique | OHSU. https://www.ohsu.edu/elemental-analysis-core/icp-ms-technique.

Optimization of DFMs (dual function materials) for combined CO_2 capture and methanation

Chloé Vandelois

Acting against climate change is one of the greatest challenges facing today's society. Greenhouse gas emissions are the main cause, leading to the emergence of a variety of solutions to mitigate them. Among these solutions, Dual Function Materials (DFMs) can both capture CO_2 and convert it into methane via its reaction with hydrogen. Allowing to produce a fuel that is both safer than hydrogen and carbon-neutral.

The properties of DFMs emerge from the simultaneous presence of basic and catalytic sites on the material. The proximity of these sites enhances reaction performance. Various compositions have been studied in the literature. In this work the DFM studied is $6\%Na_2O$-$5\%Ru/\gamma$-Al_2O_3, synthesized via two successive wet impregnations.

This work focuses on the optimization of the DFM via two axes, the synthesis process and the composition. First, different calcination temperatures were tested for ruthenium impregnation. The objective was to understand the impact of calcination temperature on dispersion and Ru particle size and its impact on catalytic performance of the resulting DFM. Then the effect of ruthenium loading was tested.

To characterize the samples, N_2 physisorption, XRD, CO_2 TPD and in situ DRIFTS measurements were carried out. For each sample, a catalytic testing was carried out to test their performance in converting CO_2 to methane using a MS setup.

Our results show that higher calcination temperature favors bigger particle size but catalytic testing shows that calcination temperature and particle size only has a marginal impact on catalytic performances. Concerning Ru loading, better performances are observed for higher Ru loadings.

UNIVERSITÉ CATHOLIQUE DE LOUVAIN
Faculté des bioingénieurs
Croix du Sud, 2 bte L7.05.01, 1348 Louvain-la-Neuve, Belgique | **www.uclouvain.be/agro**